

Article

Analysis of Fluid Field in Fish Tank of Breeding Vessel with Perforated Broadships under Wave Conditions

Wenhua Wang *, Min Li, Guoqiang Fan, Kedong Zhang  and Yi Huang

School of Naval Architecture, Dalian University of Technology, Dalian 116024, China

* Correspondence: wangwenhua@dlut.edu.cn

Abstract: For a fish tank of breeding vessels with perforated broadships, in order to analyze its fluid characteristics under wave conditions, this paper presents a numerical method and predicts the fluid field in a fish tank with opening holes. Therein, three critical problems were solved, which include wave generation, the fluid–structure interaction of waves and vessel motion, and the sloshing phenomenon in the tank. The feasibility of the method was validated through a comparison with theoretical and experimental results. On this basis, the fluid characteristics in the fish tank of a fixed breeding vessel with opening holes on side walls were discussed. Firstly, the effects of wave direction, wave height, and wave period on the flow field in the tank were mainly analyzed. Next, the fluid characteristics in the tank of a floating vessel with opening holes equipping a multi-point mooring system were investigated. Finally, the influence of motion responses of breeding vessels on the fluid field in the fish tank was examined.

Keywords: breeding vessel; fish tank; opening hole; wave conditions; fluid–structure interaction motion; sloshing phenomenon



Citation: Wang, W.; Li, M.; Fan, G.; Zhang, K.; Huang, Y. Analysis of Fluid Field in Fish Tank of Breeding Vessel with Perforated Broadships under Wave Conditions. *J. Mar. Sci. Eng.* **2024**, *12*, 367. <https://doi.org/10.3390/jmse12030367>

Academic Editor: Abdellatif Ouahsine

Received: 19 January 2024

Revised: 16 February 2024

Accepted: 19 February 2024

Published: 21 February 2024



Copyright: © 2024 by the authors. Licensee MDPI, Basel, Switzerland. This article is an open access article distributed under the terms and conditions of the Creative Commons Attribution (CC BY) license (<https://creativecommons.org/licenses/by/4.0/>).

1. Introduction

With the continuous advancement of marine aquaculture in the deep sea, large-scale equipment is being increasingly used as part of deep-sea aquaculture engineering. One example is breeding vessels that have been modified from large old ships. The cargo hold is transformed and upgraded into a fish tank, and the aquaculture system is equipped with a breeding vessel. For this equipment, its transformation cycle is short and the cost is low. Meanwhile, it has strong maneuverability and flexibility, which can conveniently select suitable aquaculture areas and avoid rough sea conditions. Thus, breeding vessels with perforated broadships (i.e., opening holes) are receiving more and more attention.

Up to now, the sizeable ship-type breeding vessels have gone through the process from conceptual design to initial engineering application. Yu and Liu (2016), Yan et al. (2016), and Sun (2019) proposed patents of modified breeding vessels [1–3]. Therein, Yu and Liu proposed a deep-water fish-farming working boat including tanks, breeding cages, and so on. Yan et al. provided a fish-farming working boat for oil tanker transformation. Sun disclosed an offshore aquaculture facility based on the transformation of bulk carriers. Furthermore, Li et al. (2015) took a 52,500 t crude oil tanker to be transformed into a breeding ship [4,5]. Its hydrostatic force and stability were estimated, and the results showed that the stability of the vessel can meet the requirements and had a certain stability reserve. Furthermore, its feasibility of application in the South China Sea has been demonstrated. Zhang et al. (2018) established the modification model of bulk carriers and developed an economic demonstration system based on the technical economy [6]. Combining the design methods of commercial transport vessels with the technical requirements of aquaculture, Cui et al. (2019) preliminarily discussed the construction of a deep-sea aquaculture ship system and overall technical framework, and proposed the technical directions that need special attention [7]. Then, Cui et al. (2020) analyzed the rapidity and power system of

a breeding vessel of 100,000 tons by means of the CFD (Computational Fluid Dynamics) method [8]. Wang et al. (2020) analyzed the process from basic structural design to strength check by the direct calculation method [9], and then carried out the basic structure design of a large breeding vessel in a manner similar to that of a double-hull oil tanker, which provides a reference for the design of this kind of ship [10]. Han et al. (2020) combined the operating characteristics of the breeding vessel and the relevant specifications of ship design and preliminarily established the stability design criteria of large-scale aquaculture vessels [11]. On this basis, some schemes are applied to practical projects (such as “Min de”, “Guoxin No. 1”, and so on), as shown in Figure 1.



(a) Min de

(b) Guoxin No. 1

Figure 1. Practical projects of breeding vessels with perforated broadside.

Generally, the broadside bulkheads of oil tankers and bulk carriers were perforated, and the cargo holds were reformed into fish tanks. Then, a series of aquaculture equipment systems were equipped to complete the transformation of the breeding vessels. When the vessel is subjected to environmental loads, the fish tank should produce periodic motions with the vessel, which causes the fluid field to generate the complex sloshing phenomenon. Moreover, side holes can make the inside and outside of the tank directly connected. Then, the external wave and current can freely enter the tank through opening holes and further enhance the complexity of water flow in the tank, which may affect the aquaculture environment of the fish tank and the survival rate of aquatic products. Therefore, it is of great engineering significance to carry out numerical simulation research on the flow field in a fish tank with open side holes.

For breeding vessels, the existing studies mainly focused on the numerical simulation of the sloshing problem in the fish tank. Labatut et al. (2015) studied the fluid field in circular and square breeding ponds by using the 3-D CFD numerical method [12]. Song et al. (2018) analyzed the relationship between the flow field at the bottom and the inlet velocity of the fish tank by CFD technology [13]. On this basis, the heat transfer and flow field in the fish tank were simulated, and the optimal inlet velocity can be determined. Cui et al. (2020) preliminarily discussed the system and overall technical framework of deep-sea aquaculture engineering equipment and studied the characteristics of the flow field in a fish tank under roll motion [14]. Then, the flow characteristics and wall pressure in the tank under pitch motion were studied, and the method to evaluate the ability of the tank was established based on the STARCCM+ platform [15]. Then, the influence of ship motions on the sloshing phenomenon in the tank was analyzed based on the CFD method. Xiao et al. (2020) investigated the coupled effects between the sloshing fluid in the tank and the motion responses of the vessel and discussed the influence of the shear force on the sloshing phenomenon, which can provide a reference for the optimal design of the aquaculture vessel by using the Fluent platform [16,17]. Xu and Yang (2017) studied the sloshing problem in fish tanks and discussed the water velocity in the tank under different anti-sloshing methods based on CFD theory [18]. Gao et al. (2020) used the flow rate as the evaluation standard and analyzed the effects of the roll motion of the vessels on the fish adaptability from anti-sloshing methods, tank type, and external excitation [19]. Fang et al. (2021) discussed a numerical calculation model of a fish tank based on the CFD technique

and analyzed the characteristics of the flow field in the tank under roll motion [20]. Wu and Chen (2021) captured the free surface in the tank by the VOF (Volume of fluid) method and simulated the effects of the fluid field in the tank on the motion responses of the vessel under practical waves with different frequencies [21]. Based on the above research about closed breeding vessels, Liu (2019) studied the characteristics of the flow field in a fish tank under the free-flowing condition of the opening hole based on a 2D fish tank with a perforated broadside by using the Fluent platform [22]. Most of the above studies focused on the sloshing problem of the fish tank with a closed state by various numerical methods and did not consider the influence of free water flow at the opening hole on the fluid field in the tank. In addition, the studies considering the perforated broadside ignored the influence of the six DOF coupling motions of the vessel. The above research conclusions were not applicable to practical 3D breeding vessels with perforated broadsides (i.e., opening holes), and thus, it is of great research value to establish a numerical method that can accurately consider the fluid sloshing caused by the bulkhead and the interactive flow due to opening holes in the fish tank of 3D breeding vessels with perforated broadsides.

For the fluid characteristics in the fish tank of breeding vessels with perforated broadsides under wave conditions, this paper presents a numerical method to predict the fluid field in the fish tank, including three critical problems of wave generation, fluid–structure interaction motion, and the sloshing phenomenon in the tank. On this basis, fluid characteristics in the fish tank of fixed breeding vessels with opening holes were discussed. Therein, the effects of wave direction, wave height, and wave period on the flow field in the fish tank were analyzed. Furthermore, the fluid characteristics in the fish tank of floating breeding vessels with perforated broadsides with a mooring system were investigated. Then, the influence of motion responses of breeding vessels on the fluid field in the fish tank was mainly discussed.

2. Establishment and Validation of Numerical Methods

2.1. Numerical Model

In the present method, the fluid field in a tank of breeding vessels with perforated broadsides under wave conditions was simulated by using the CFD method based on the STARCCM+ platform. The flow was assumed to be incompressible. Continuity equation and Navier–Stokes equations in vector form using the Cartesian coordinate system can be written as follows:

$$\nabla \cdot v = 0 \tag{1}$$

$$\rho \left(\frac{\partial v}{\partial t} + v \cdot \nabla v \right) = -\nabla p + \mu \nabla^2 v + \rho g \tag{2}$$

where v represents the velocity vector, ρ is the fluid density, p is the pressure, μ is the dynamic viscosity, ∇^2 denotes the Laplace operator, and g is the gravity acceleration.

On this basis, the RANS equations (Reynolds-averaged Navier–Stokes equations) were applied, and then the turbulent flow was numerically simulated based on the realizable k - ε model (Irkal et al., 2016; Gokce and Kinaci, 2018) [23,24]. The viscous sublayer and buffer layer of the wall area are treated with wall treatment of full y^+ .

$$\frac{\partial(\rho k)}{\partial t} + \frac{\partial(\rho k u_i)}{\partial x_i} = \frac{\partial}{\partial x_j} \left[\left(\mu + \frac{\mu_t}{\sigma_k} \right) \frac{\partial k}{\partial x_j} \right] + G_k - \rho \varepsilon \tag{3}$$

$$\frac{\partial(\rho \varepsilon)}{\partial t} + \frac{\partial(\rho \varepsilon u_i)}{\partial x_i} = \frac{\partial}{\partial x_j} \left[\left(\mu + \frac{\mu_t}{\sigma_\varepsilon} \right) \frac{\partial \varepsilon}{\partial x_j} \right] + C_{1\varepsilon} \frac{\varepsilon}{k} G_k - C_{2\varepsilon} \rho \frac{\varepsilon^2}{k} \tag{4}$$

where k stands for the turbulence kinetic energy, ε is the dissipation rate, σ_k and σ_ε are Prandtl numbers corresponding to k and ε , respectively, $C_{1\varepsilon}$ and $C_{2\varepsilon}$ are experience coefficient, and G_k is the production term of turbulent kinetic energy k caused by the average velocity gradient.

The volume of fluid (VOF) method by Hirt and Nichols (1981) was used to capture the water–air interface [25]. This method determines the volume fraction of each fluid through the following equation,

$$\frac{\partial C_q}{\partial t} + \nabla \cdot (C_q v) = 0, q = 1, 2 \tag{5}$$

where C_1 and C_2 represent the volume fraction of water and air, and their sum is one all the time.

On this basis, the wave-forcing technique was applied in the numerical method. In order to drive the solutions of the RANS equations tending to the specified regular wave, a source was introduced into the momentum conservation equation as follows.

$$q_\phi = -\gamma\rho(\phi - \phi^*) \tag{6}$$

where γ is the force coefficient, ρ is the fluid density, ϕ is the current solution of transport equations, and ϕ^* is an approximate value of the forcing method. Therein, force coefficient γ can change smoothly in the specified force area, which can take the square form of trigonometric functions. The wave-forcing method can not only effectively reduce the size of the computation domain but also eliminate the wave reflection at the boundary.

Furthermore, the numerical technique of dynamic fluid body interaction (DFBI) was used, in order to simulate six degree-of-freedom (DOF) motions of the breeding vessel. Within each time step, external wave loads were applied on the breeding vessel, and then motion equations were solved to achieve the new position and orientation of the body. Moreover, the overset mesh system was used to deal with the vessel motions with large amplitudes.

Because there are no whole model tests for the fish tank of breeding vessels with perforated broadsides under the regular wave, the key issues in the whole physical process, namely, three test cases of wave generation, fluid-structure interaction motion, and the sloshing phenomenon in the tank, were taken to validate the feasibility of the numerical method in this paper.

2.2. Numerical Tank with Wave Making and Absorbing Techniques

Here, the wave condition in the test case can be selected as a regular wave with wave height $H = 0.07$ m and wave period $T = 1.291$ s (wave length 2.61 m). The computational domain was $10 \lambda \times 0.7$ m \times 2.25 m with 1.35 m water depth. Therein, λ denotes wave length. That is to say, the longitudinal direction was taken as 10 times the wave length. The two sides for the front and back of the vessel correspond to the directions of the wave flowing in and out. The wave-forcing technique was applied and its range was taken as 1 times the wave length. Here, the x -axis was the direction of wave propagation.

In order to more accurately capture the shape of the free surface, numerical meshes were refined near the surface. Therein, the grid size in the z direction was taken as 0.0035 m (1/20 of the wave height), then the length and the width were 0.028 m (1:8 aspect ratio), as shown in Figure 2.

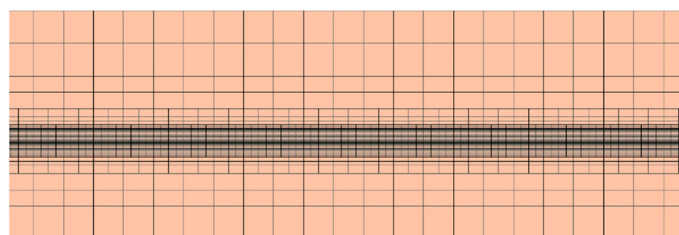


Figure 2. Refined numerical meshes near the free surface.

Firstly, the convergences of the numerical method about the mesh size and time step were verified. The grid schemes should be mainly determined based on the local mesh near

the surface, whose vertical heights include $(1/10) H$, $(1/20) H$, and $(1/30) H$. Furthermore, three different schemes with 0.005 s, 0.010 s, and 0.020 s were taken. Time histories of wave elevation at classic monitoring points were numerically calculated and are shown in Figure 3.

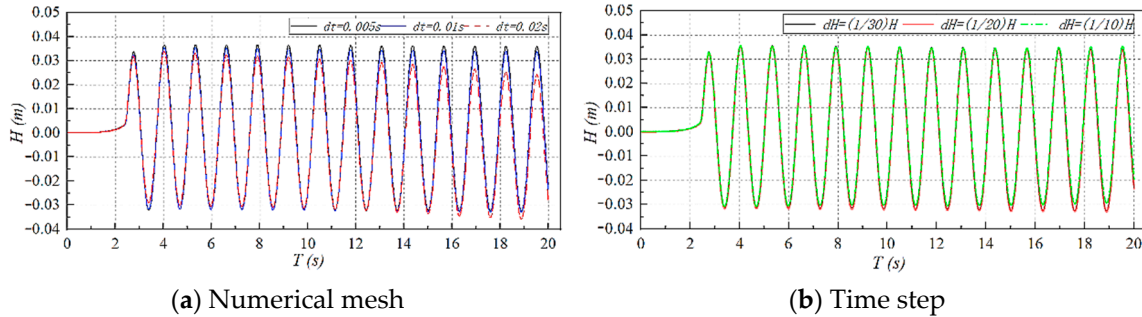


Figure 3. Convergence of the method about numerical mesh and time step.

From the figure, it can be found that the numerical results between $(1/20) H$ and $(1/30) H$ are very close, which is mainly different from that of $(1/10) H$. Furthermore, with the time step decreasing from 0.020 s to 0.005 s, numerical results of wave elevation become stable gradually. By considering the computational precision and efficiency, the numerical scheme with $(1/20) H$ (size of numerical mesh) and 0.010 s (time step) was applied for the numerical wave tank.

On this basis, wave contour can be numerically simulated, as shown in Figure 4. Then, the results by the numerical and theoretical wave heights can be compared, as shown in Figure 5 and listed in Table 1. It can be seen that the relative error of the numerical result and theoretical solution is 4.28%, which can meet the engineering precision requirements and thus show that the numerical method is accurate enough to simulate the classic wave condition.

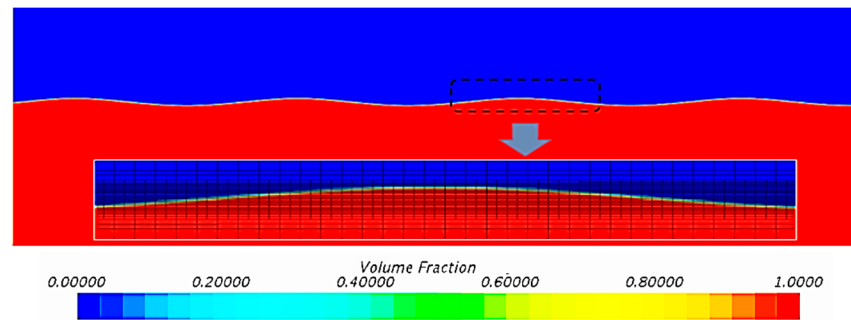


Figure 4. Wave contour in numerical wave tank.

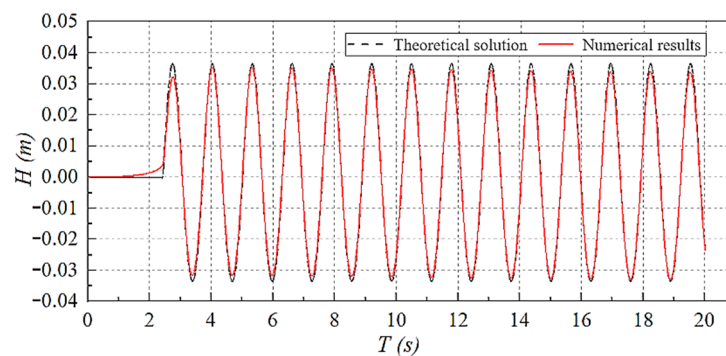


Figure 5. Validation of the numerical method to predict the classic wave condition.

Table 1. Comparison of the numerical result and theoretical solution of wave height.

	Unit	Theoretical Solution	Numerical Result	Relative Error
Wave height	m	0.070	0.067	4.28%

2.3. Fluid–Structure Interaction Method on Motion Responses of Breeding Vessels in Wave

In this section, the scale model of a breeding vessel with a scale ratio of 1:60 was created, as shown in Figure 6, whose main parameters can be listed in Table 2.

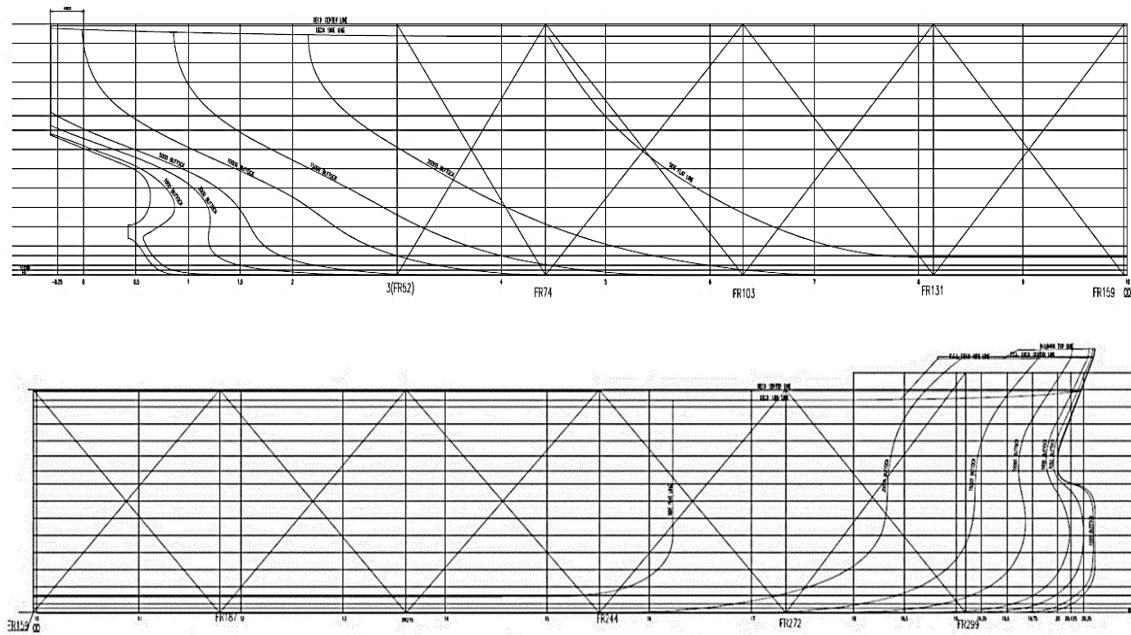


Figure 6. Longitudinal profile of a breeding vessel.

Table 2. Main parameters of the breeding vessel.

Main Parameter	Unit	Practical Model	Scale Model
Main length	m	291.80	4.86
Width	m	45.00	0.75
Displacement	t	236,469.70	1.09
Draught	m	21.00	0.35
Longitudinal position of COG	m	148.35	2.43
Vertical position of COG	m	11.55	0.19
Roll inertia radius	m	13.70	0.23
Pitch inertia radius	m	70.90	1.18

Based on line plans and main parameters, three-dimensional numerical and experimental models of the breeding vessel can be obtained as shown in Figure 7. Furthermore, wave parameters of classic regular waves are listed in Table 3. Therein, wave steepness (H/λ) denotes the ratio of wave height H and wave length λ . The experimental tests were performed in the state key laboratory of coastal and offshore engineering of Dalian University of Technology. Therein, the integrated multifunctional pool, wave height measuring instrument, and noncontact motion measurement system were used in the experiments. In the integrated multi-functional pool, the wake-making and absorbing systems are equipped for various regular and irregular wave experiments, including the experiments of two classic regular waves in this research. Moreover, the wave height measuring instrument can be used to obtain the time history of wave elevation, which is based on the principle of resistance. The theoretical basis of its design is that the resistance in water changes linearly

with the variation in water level. Finally, the non-contact motion measurement system is based on the stereo vision theory and can be applied to achieve the position information of the floating model by the digital image processing technique.

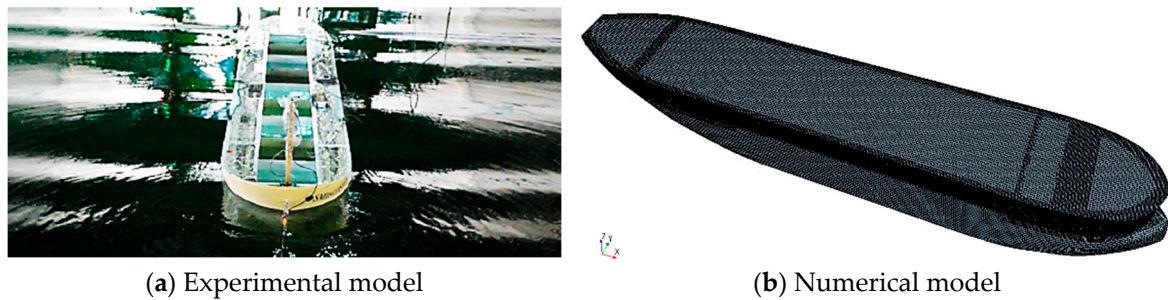


Figure 7. Numerical and experimental models of the breeding vessel.

Table 3. Wave parameters of classic regular waves.

Case	Wave Height H (m)	Wave Period T (s)	Water Depth d (m)	Wave Length λ (m)	Wave Steepness (-)
A	0.070	1.291	1.267	2.610	1:37
B	0.070	1.936	1.267	5.852	1:84

The main body of the vessel was made of fiberglass and wood, whose COG and inertia moment were achieved by adjusting the weight and position of iron ballasts, in order to ensure that the displacement and mass distribution of the model were similar to that of the practical vessel.

The numerical computational domain and boundary conditions were created as shown in Figure 8. The computational domain was $10 \lambda \times 6 \lambda \times 2.25$ m with 1.35 m water depth; that is to say, the longitudinal and transverse sizes were taken as 10 times and 6 times the wave length, respectively. On all four side faces around the computational domain, wave-forcing zones with 1λ length were applied.

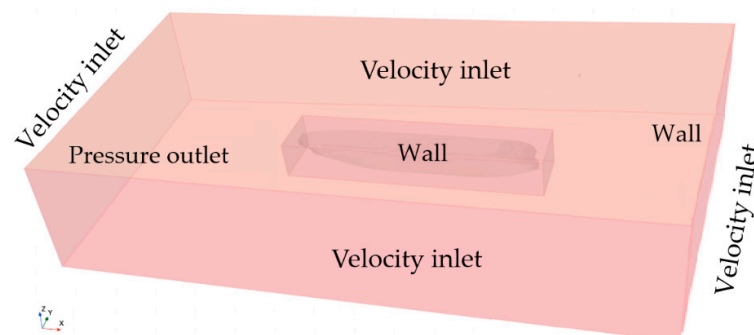


Figure 8. Boundary conditions for the case of the breeding vessel without opening holes.

Numerical meshes on classic longitudinal and transverse sections in the computational domain were generated in Figure 9a. The total numerical meshes were about 475 million. Moreover, two-phase distribution and wave surface can be numerically simulated and shown in Figure 9b, and then the heave and pitch motion responses of a scale breeding vessel were plotted, as shown in Figures 10 and 11.

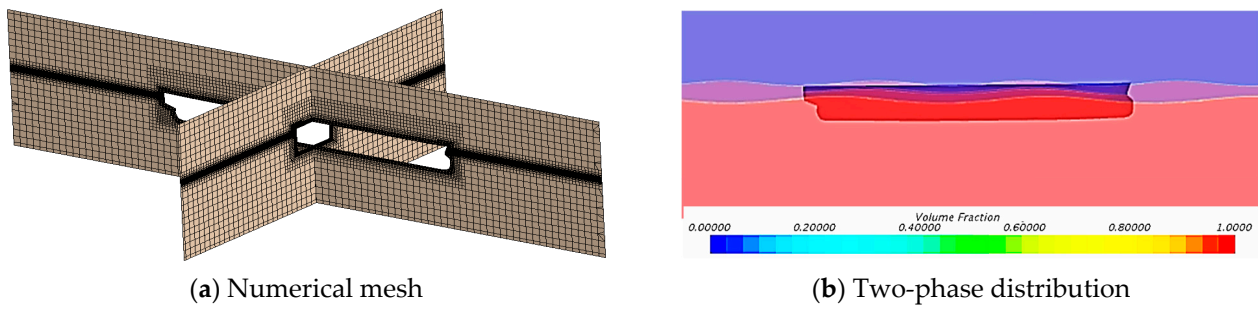


Figure 9. Numerical mesh and two-phase distribution to numerically simulate motions of the breeding vessel in wave.

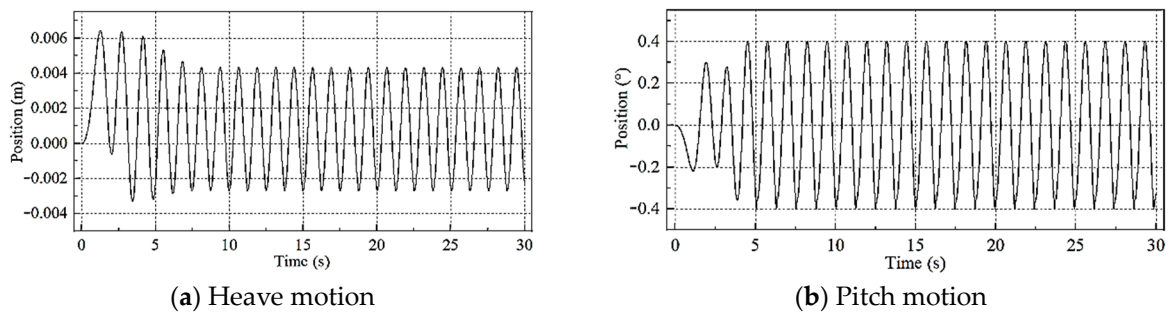


Figure 10. Time histories of heave and pitch motion responses in the wave condition of case A.

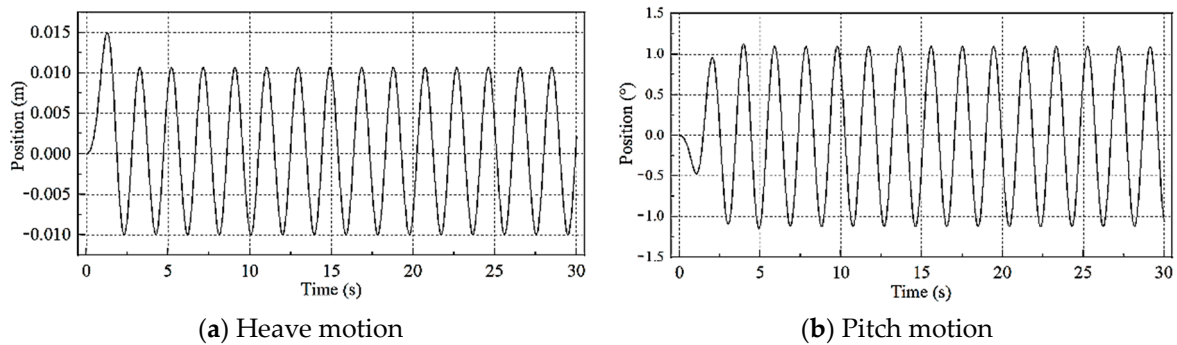


Figure 11. Time histories of heave and pitch motion responses in the wave condition of case B.

For wave conditions of case A and case B, the numerical and experimental results were obtained and comparatively analyzed in Table 4. From the table, it can be found that the relative errors of numerical results and experimental solutions are within 10%, which shows the feasibility of the method in predicting the motion response of the breeding vessel in waves.

Table 4. Comparison of numerical and experimental motion responses of the breeding vessel.

Case	Heave Motion (m)			Pitch Motion (deg)		
	Numerical Method	Experimental Method	Relative Error	Numerical Method	Experimental Method	Relative Error
A	0.0035	0.0034	2.06%	0.3969	0.3770	5.29%
B	0.0103	0.0113	−8.70%	1.1004	1.0735	2.50%

2.4. Numerical Method to Simulate Sloshing Phenomenon in Tank Due to Bulkhead Motion

For the sloshing phenomenon due to the motion of the tank, here, the test case by Faltinsen (1978) was performed in Figure 12, in order to validate the numerical method of

this paper. Numerical meshes in the tank were created, as shown in Figure 13a, and initial phase contour and free surface were set up, as shown in Figure 13b. The total numerical meshes were about 10,000.

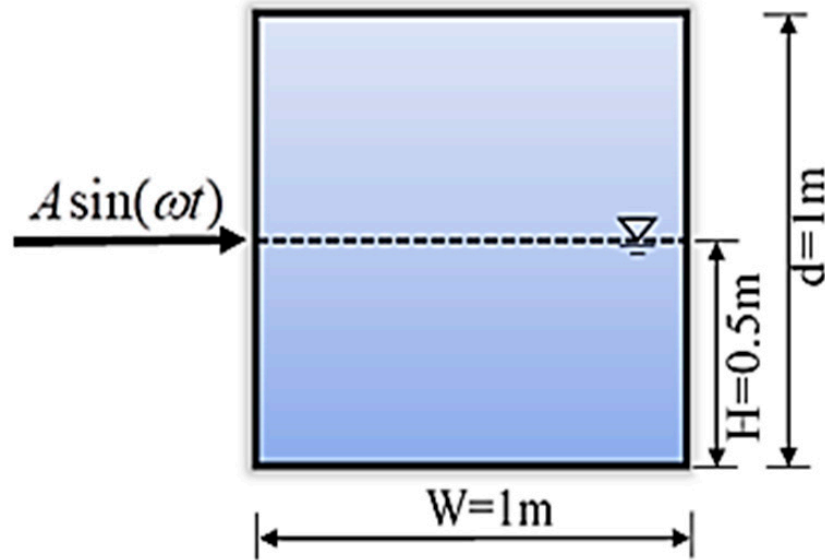


Figure 12. The test case to validate sloshing phenomenon.

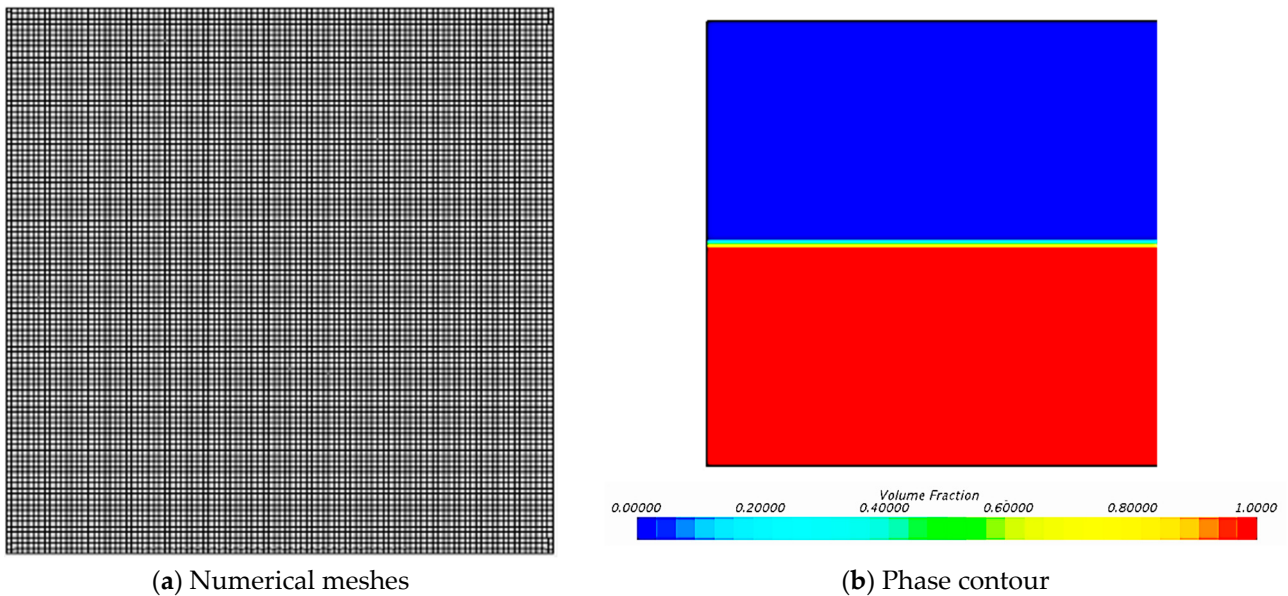


Figure 13. Numerical meshes and initial phase contour in the tank.

Here, two cases of the tank with sway motion ($x = A \sin \omega t$) of different amplitudes and periods were taken, including case 1 ($A = 0.01\text{ m}$, $\omega = 2.655\text{ rad/s}$) and case 2 ($A = 0.0004\text{ m}$, $\omega = 5.045\text{ rad/s}$). Surface heights at the midpoint of the right bulkhead were numerically calculated and are shown in Figure 14. It can be seen that the numerical results are in agreement with the theoretical solutions, which shows that the numerical method can accurately simulate the characteristics of the sloshing surface in the tank. Furthermore, in the case that motion frequency is close to the natural frequency of 5.31 rad/s , the unstable surface elevation can be greatly simulated by means of the numerical method.

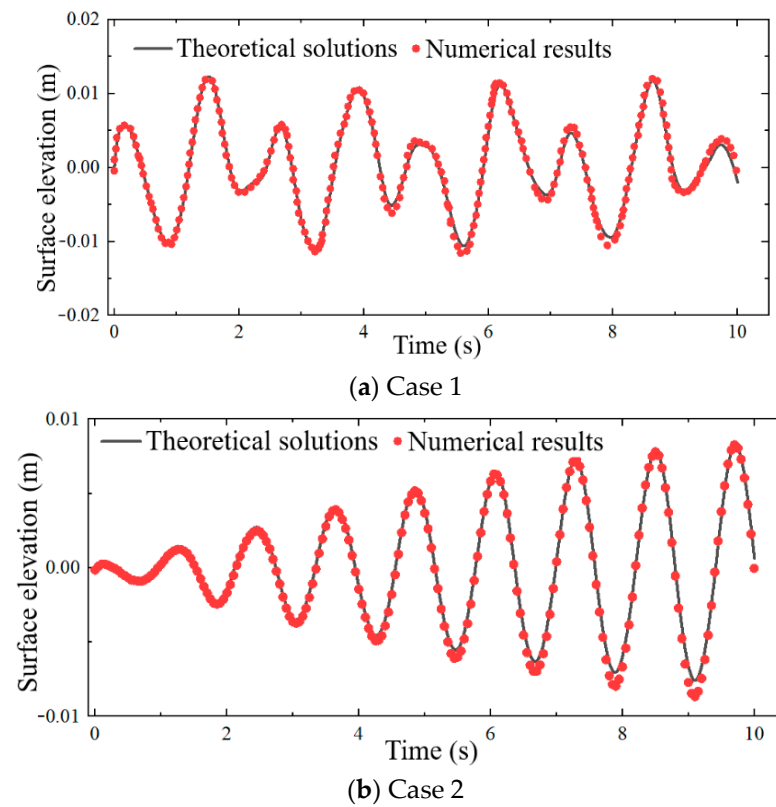


Figure 14. Time histories of surface elevation at the midpoint of right bulkhead.

3. Results and Discussions

In this section, the fluid characteristics in the fish tank of the breeding vessel with perforated broadsides under various wave conditions were discussed. Therein, the main parameters of the tank are listed in Table 5, and its geometrical model and opening holes (# R_1 – R_5 on the right-side wall and # L_1 – L_5 on the left-side wall) are shown in Figure 15.

Table 5. Main parameters of fish tank.

Parameters	Unit	Practical Model	Scale Model (1:60)
Tank width	m	44.40	0.740
Tank height	m	22.25	0.371
Hole diameter	m	2.00	0.033
Water height	m	18.55	0.309
Distance of hole	m	0.10	0.00167

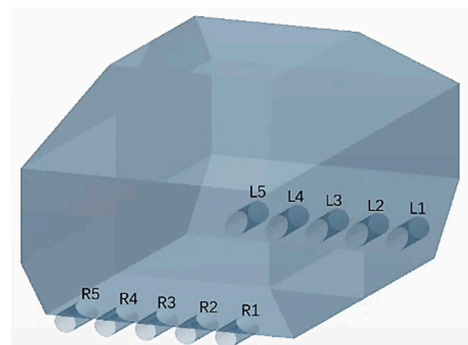


Figure 15. Geometrical model and monitoring points.

Here, the computational domain was $10 \lambda \times 6 \lambda \times 2.25 \text{ m}$ with 1.35 m water depth; that is to say, the longitudinal and transverse sizes were taken as 10 times and 6 times the wavelength, respectively. On all four side faces around the computational domain, wave-forcing zones with 1λ length were applied. Boundary conditions of the computational domain are shown in Figure 16. According to the main parameters of the vessel, the zone of overset mesh was taken as $5.2 \text{ m} \times 1.0 \text{ m} \times 0.6 \text{ m}$, which can effectively contain the vessel model.

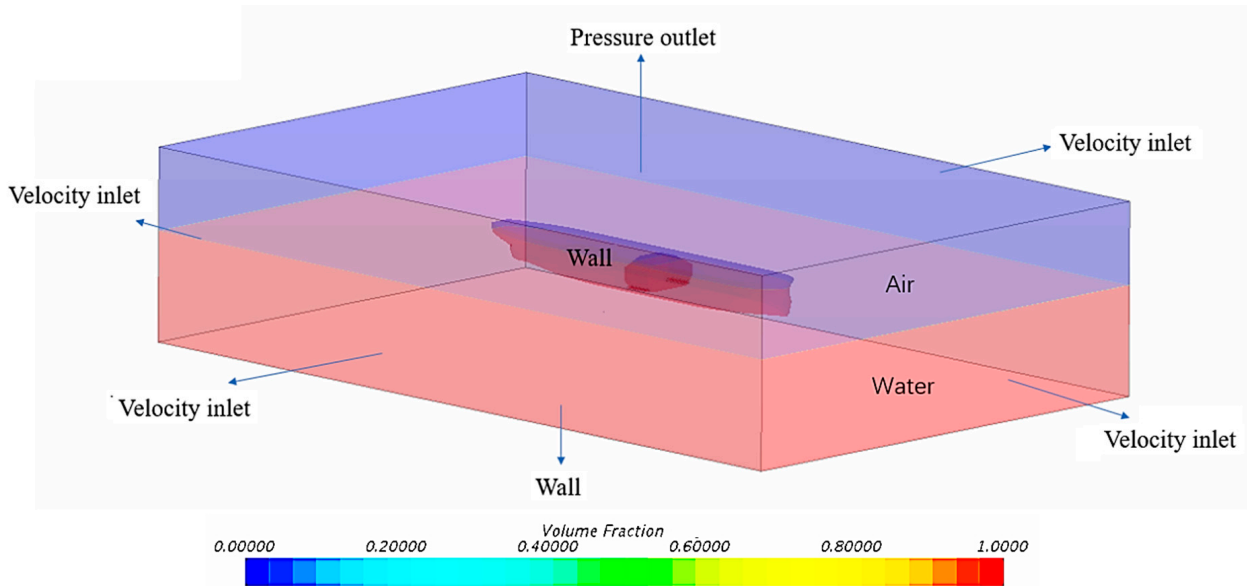
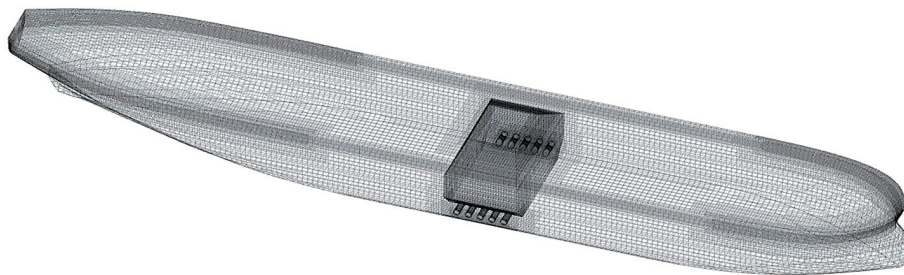
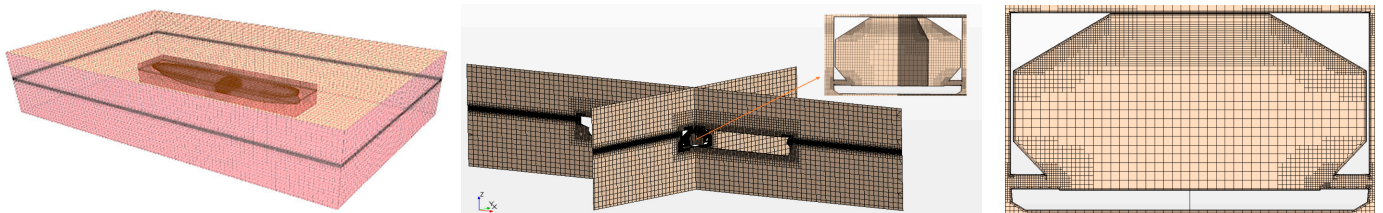


Figure 16. Boundary conditions for the case of the breeding vessel with perforated broadside.

Then, the case of the fish tank in the middle of the vessel was taken. The arrangement of the fish tank and the numerical model of the breeding vessel with the fish tank are shown in Figure 17a. Then, the computational domain can be numerically discretized in Figure 17b. The total numerical meshes were about 480 million.



(a) Numerical model of the breeding vessel with fish tank



(b) Numerical meshes of computational domain

Figure 17. Numerical meshes of the breeding vessel and fish tank in computational domain.

3.1. Fluid Characteristic in Fish Tank of a Fixed Breeding Vessel with Perforated Broadside

Firstly, here, the breeding vessel was fixed in a numerical simulation in order to neglect the effect of vessel motions on the fluid field in a fish tank, in order to mainly analyze the process of different waves entering the fish tank through opening holes. Therein, the effects of various wave parameters on the fluid field in the tank were discussed.

3.1.1. Influence of Wave Direction on Flow Field in the Fish Tank

Three wave conditions with various directions are discussed in Table 6. Therein, 90° denotes the condition of a beam sea, 135° is oblique propagation from the ship bow, and 180° means head sea from the bow. According to the parameters, the fifth-order Stokes wave theory was applied here. Then, time histories of average flow flux at various opening holes versus different wave directions were calculated and shown in Figure 18.

Table 6. Main parameters of wave conditions with different directions.

Case	Wave Direction	Wave Height H (m)	Water Depth D (m)	Wave Period T (s)	Wave Length λ (m)
A	90°	0.070	1.267	1.291	2.610
B	135°	0.070	1.267	1.291	2.610
C	180°	0.070	1.267	1.291	2.610

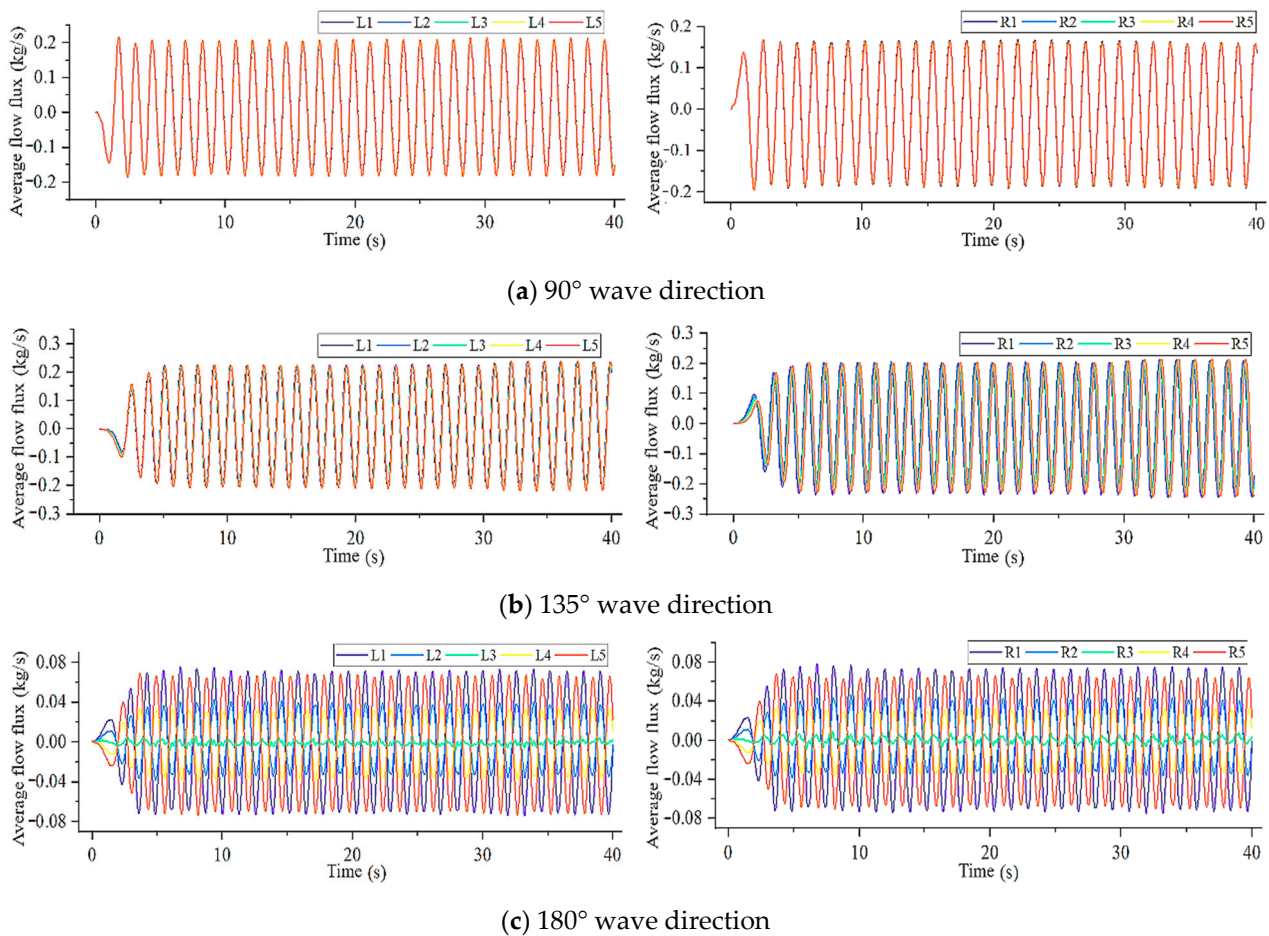


Figure 18. Time histories of average flow flux at various holes versus different wave directions.

From the figure, each time-domain curve of average flow flux at different opening holes has a trend of periodic variation. For the condition of the wave direction 90° , the average flux of each hole at the same moment is basically the same. When the wave

direction is 135°, which is inclined relative to the vessel, the wave travels first to hole R_1 and finally to hole R_5 . Thus, there are phase differences in the flow flux versus different opening holes on the side facing the wave at the same time. Moreover, the flux of each hole for the wave direction 180° is very different from that of the above two wave directions. The differences mainly lie in the following two aspects. On one hand, a wave with the 180° direction propagates from bow to stern, and the exchange of water inside and outside the tank through opening holes is small, which causes the flux to be minimal. On the other hand, during the process of wave propagation, the fluid first flows into the fish tank through $R_1, L_1, R_2,$ and L_2 and then flows out of $R_4, L_4, R_5,$ and L_5 , which leads to the phase alternations of the flow flux of each hole in Figure 18c.

Because the flow flux through holes for the 180° wave direction is much smaller than that of 135° and 90°, the flux of 135° was only compared with that of 90°. Then, the total inflow and outflow within 20–30 s were listed in Table 7. It can be seen that the inflow and outflow are basically the same, indicating that the water volume in the tank is basically consistent. Furthermore, the total inflow and outflow under the 135° wave are about 15% larger than those under the 90° wave, which shows that the exchange of water inside and outside the tank is more significant in the case of the 135° wave.

Table 7. Total inflow and outflow through opening holes versus different wave conditions.

Wave Direction	Total Inflow (kg)	Total Outflow (kg)	Relative Difference
90°	5.446	−5.532	1.58%
135°	6.420	−6.454	0.53%
Relative difference	15.17%	14.29%	-

Subsequently, the evolution process of fluid fields in the fish tank under 90° and 135° wave conditions was numerically simulated, as shown in Figures 19 and 20.

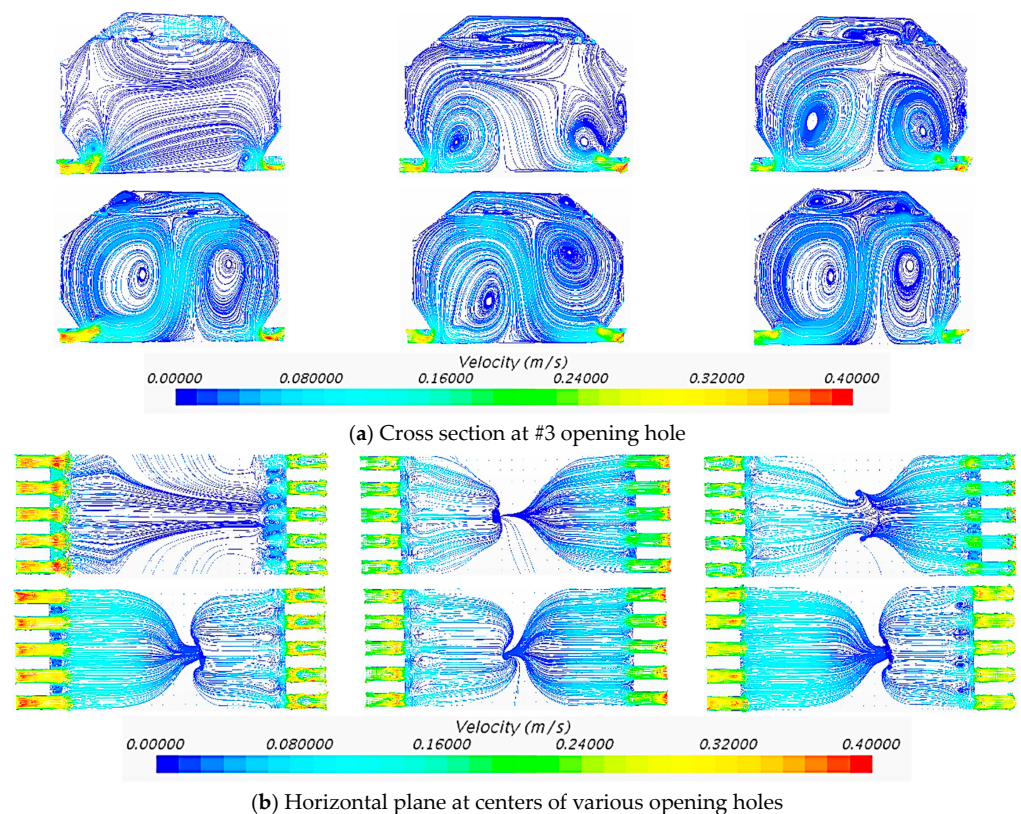


Figure 19. Streamline in the fish tank under 90° wave at classic moments (from left to right, from top to bottom: 2.0 s, 9.0 s, 13.0 s, 35.5 s, 36.0 s, and 36.5 s).

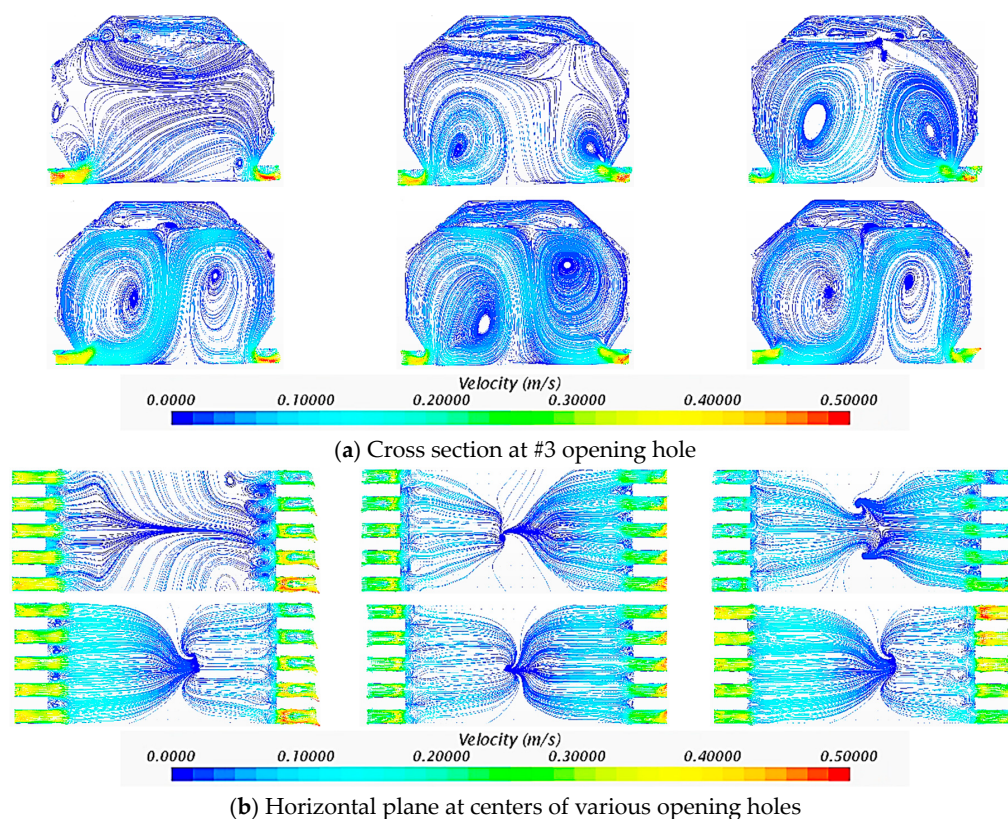


Figure 20. Streamline in fish tank under 135° wave at classic moments (from left to right, from top to bottom: 2.0 s, 9.0 s, 13.0 s, 35.5 s, 36.0 s, and 36.5 s).

From Figure 19, under the 90° wave, as time advances, the fluid field in the tank and the flow flux through the holes gradually tend to stabilize periodically with waves. The opening holes are arranged on both sides near the bottom of the tank, so the incoming flow first affects the fluid field in the lower part of the tank and diffuses throughout the horizontal plane at $t = 2.0$ s. When the flow at the opening hole is in the outflow state, a small vortex is generated near the hole due to the adsorption effect during the outflow process. Next, until the opening is in the inflow state, external fluid will flow into the tank under the vortex, causing it to move upward and disperse into several smaller vortices. With the gradual inflow of fluid, the vorticity field strengthens and gradually forms two large-scale vortices near both sides at $t = 9.0$ s and 13.0 s. The fluid entering the tank flows below the vortex near the inlet first and then follows the motion mode of the vortex toward the top of the vortex on the other side. Furthermore, the disturbance range of the flow field in the horizontal plane is mainly between two holes of #1 and #5, and the phenomenon of fluid accumulation toward the middle #3 hole is produced. Next, with the vortex tending to the steady state from $t = 35.5$ s to 36.5 s, the fluid arrives at the outlet hole and divides into two directions. Part of the fluid flows out of the tank through the opening hole, and the other part continues to move with the vortex, which gradually increases the vortices on both sides and drives the fluid inside the tank to flow alternately. Therein, near the hole with the outflow state, the location of the vortex core on the side is lower, and the location of the core on the side of the inflow state is higher, which reflects the periodic change in the motion state of the vortex.

From Figure 20 under the 135° wave condition, it can also be found that the inflow and outflow process of the fluid through holes on the left and right sides also has periodic characteristics. The evolution process of 135° is basically the same as the 90° condition. From the two figures, after the flow field becomes stable, the overall vortices in the cross-section of #3 and local vortices near holes on the horizontal plane in the tank for the 90° case are more significant than that of 135° due to the two directions through the inlet holes,

which can have the effect of hindering the flow exchange. Thus, the flow velocities under the 135° wave are more significant than those under the 90° wave, which can effectively prove the conclusion of Table 7 that the exchange rate under the 135° wave is greater.

The streamline of the stable fluid field in the tank under the 180° wave was simulated, and is plotted in Figure 21. For this case, its inflow and outflow patterns are different from 135° and 90°. The external wave propagating along the vessel surface flows into the fish tank, which drives the fluid in the fish tank to move forward and backward, and then finally converges at the location of the #3 hole in the middle of the tank, which causes the convergent fluid to flow upward, leftwards and rightwards, forming horizontal and vertical vortices. From Figure 21a, the streamline on the classic cross-section is stable in the form of two vortices on the left and right. From Figure 21b, the streamline on the classic horizontal plane presents a regular changing trend with periodic vortex.

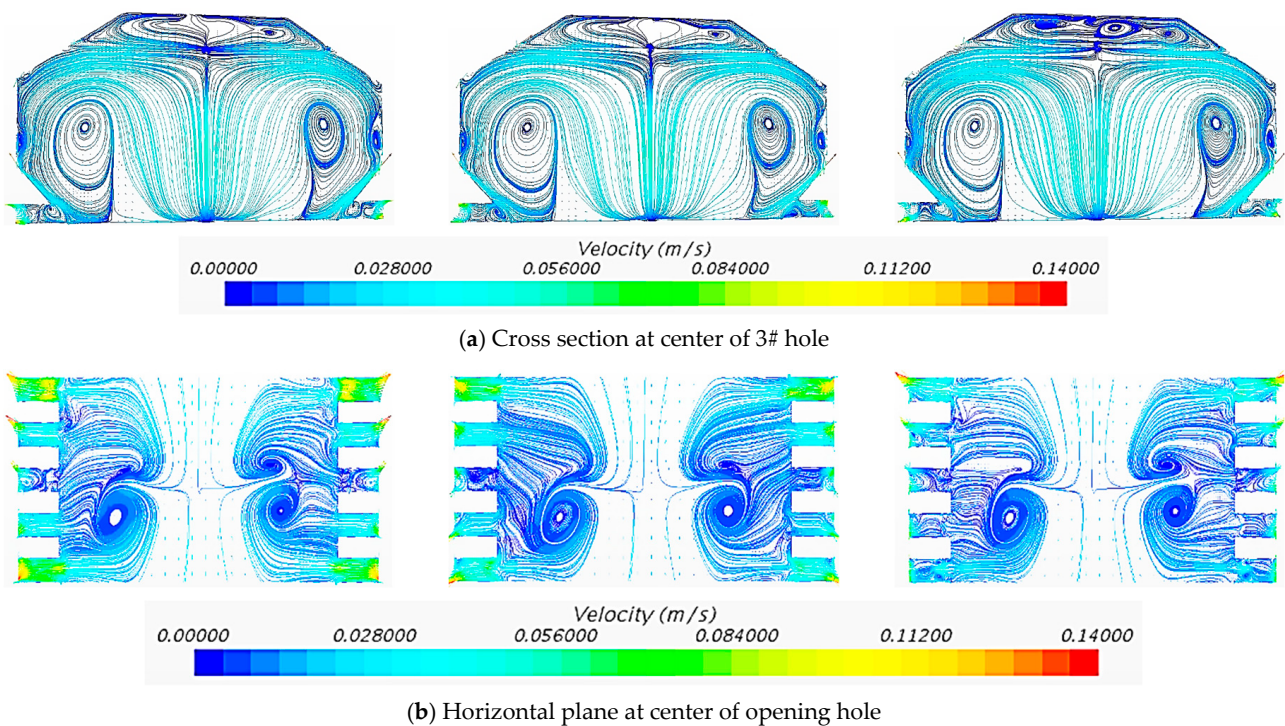


Figure 21. Streamline of fluid field in fish tank under 180° wave condition (38.5 s, 39.0 s, and 39.5 s).

3.1.2. Influence of Wave Height on Flow Field in Fish Tank

Here, two wave conditions with different heights were studied as listed in Table 8, and fifth-order Stokes wave theory was used. Therein, wave steepness (H/λ) denotes the ratio of wave height H and wave length λ . The numerical results of case B are referred to in Figure 18a in Section 3.1.1. Then, case A with wave height 0.05 m was numerically simulated, and its time histories of average flow flux at various holes are shown in Figure 22. From the figure, it can be seen that periodic-variational curves of the average flow rate at five openings on the same side are consistent. Furthermore, average flow fluxes of 0.05 m and 0.07 m wave heights at opening holes of R_3 and L_3 were compared and shown in Figure 23. As shown in the figure, the amplitude of the average flow flux becomes greater with the increase in the wave height, which also means that the larger the wave height is, the greater the flow exchange between the fluid field in the tank and the external environment. Meanwhile, the wave with a larger height should cause the vortex flow in the tank to become more pronounced, as shown in Figure 24.

Table 8. Main parameters of wave conditions with different heights.

Case	Wave Direction	Wave Height H (m)	Water Depth D (m)	Wave Period T (s)	Wave Length λ (m)	Dimensionless Wave Length (-)	Wave Steepness (-)
A	90°	0.050	1.267	1.291	2.610	0.54	1:52
B	90°	0.070	1.267	1.291	2.610	0.54	1:37

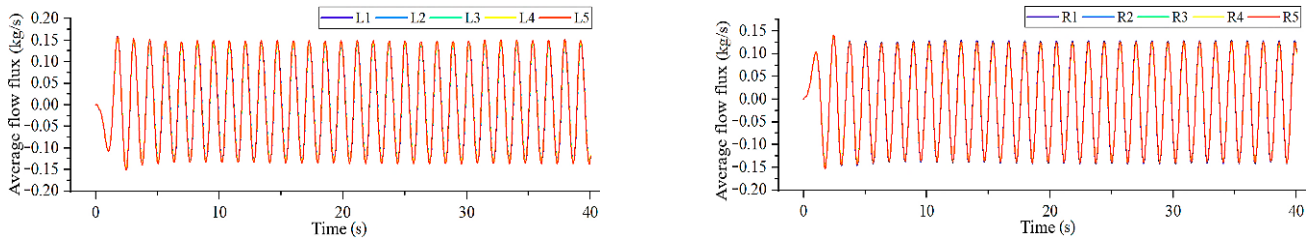


Figure 22. Time histories of average flow flux at various opening holes with 0.05 m wave height.

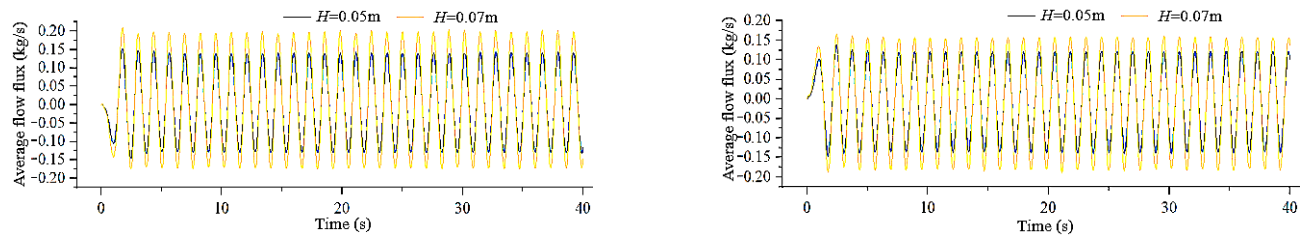


Figure 23. Comparison of flow fluxes through #3 hole versus wave heights of 0.05 m and 0.07 m.

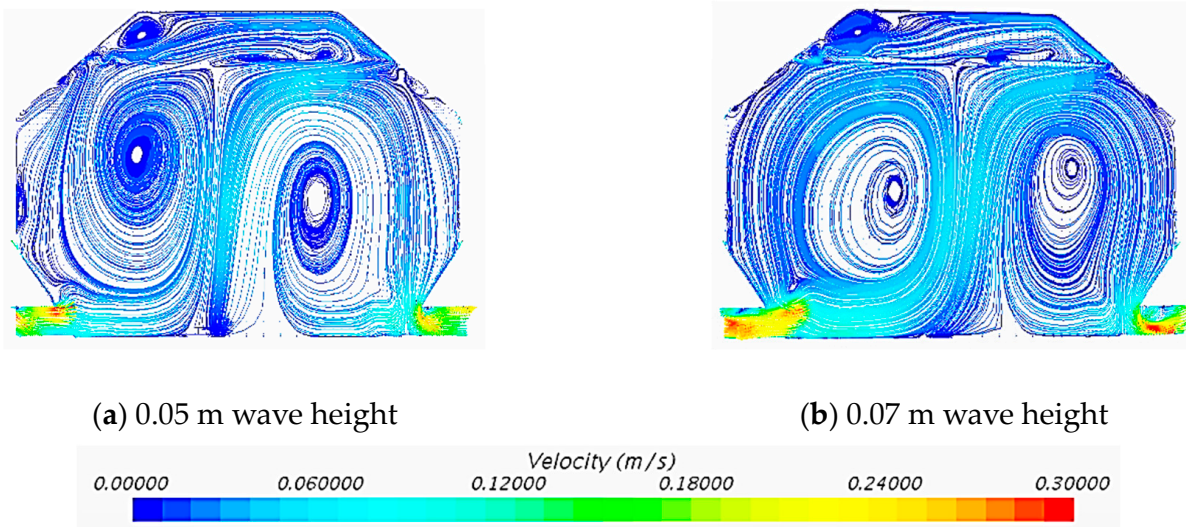


Figure 24. Comparison of vortexes in the tank versus different wave heights of 0.05 m and 0.07 m.

3.1.3. Influence of Wave Period on Flow Field in the Fish Tank

Here, three wave conditions with various periods are analyzed in Table 9, and 5th Stokes wave theory was taken. Therein, wave steepness (H/λ) denotes the ratio of wave height H and wave length λ . The numerical solutions of case C are referred to in Figure 18a in Section 3.1.1. Then, case A with period 0.646 s and case B with period 1.033 s were numerically calculated, and their time histories of average flow flux at various holes are plotted in Figure 25.

Table 9. Main parameters of wave conditions with different periods.

Case	Wave Direction	Wave Height H (m)	Water Depth D (m)	Wave Period T (s)	Wave Length λ (m)	Dimensionless Wave Length (-)	Wave Steepness (-)
A	90°	0.070	1.267	0.646	0.715	0.14	1:10
B	90°	0.070	1.267	1.033	1.693	0.35	1:24
C	90°	0.070	1.267	1.291	2.610	0.54	1:37

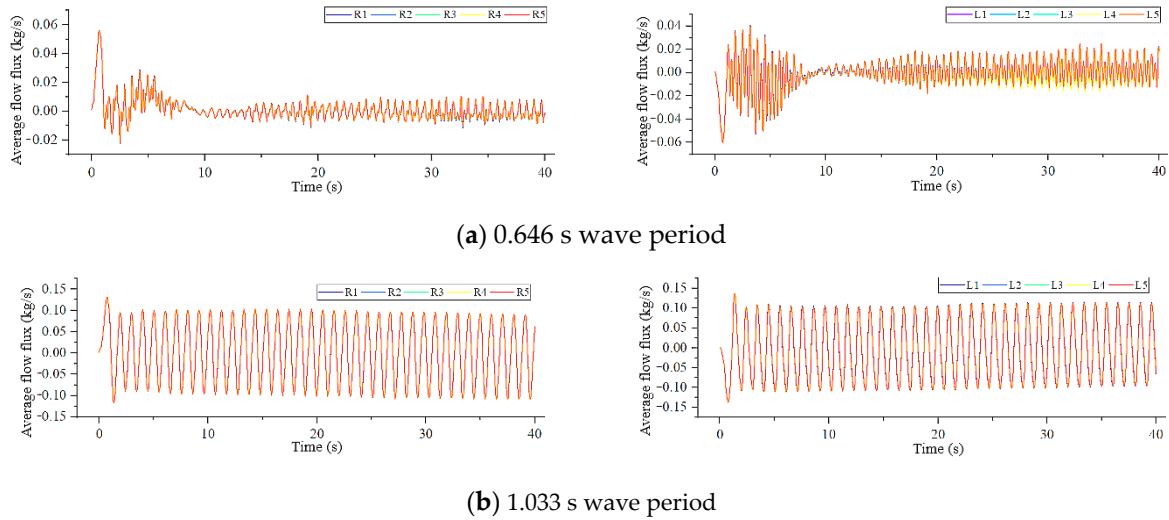


Figure 25. Time histories of average flow flux at various opening holes versus different wave periods.

From Figure 25, firstly the irregular characteristics of flow flux for a 0.646 s wave period can be found. Thus, taking the time-history curve of flow flux at the L_1 hole for example, the flow flux from 20 s to 50 s is plotted in Figure 26a. From the figure, it can be found that the curve exhibits irregular periodicity. Then, the FFT method can be used to analyze the frequency characteristics, as shown in Figure 26b. For the wave with a 0.715 m wave length and 0.646 s wave period, the wave frequency should be 9.72 rad/s. The first-order natural frequency should be excited and, thus, the first peak should occur at about 9.43 rad/s. Then, twice the wave frequency should be 19.44 rad/s, which is very close to the four-order natural frequency of about 18.86 rad/s. Therefore, the second super-harmonic resonance of the fluid motion in the fish tank should be excited. Then, the second peak of the flow flux is located at a frequency of 18.87 rad/s, as shown in Figure 26b.

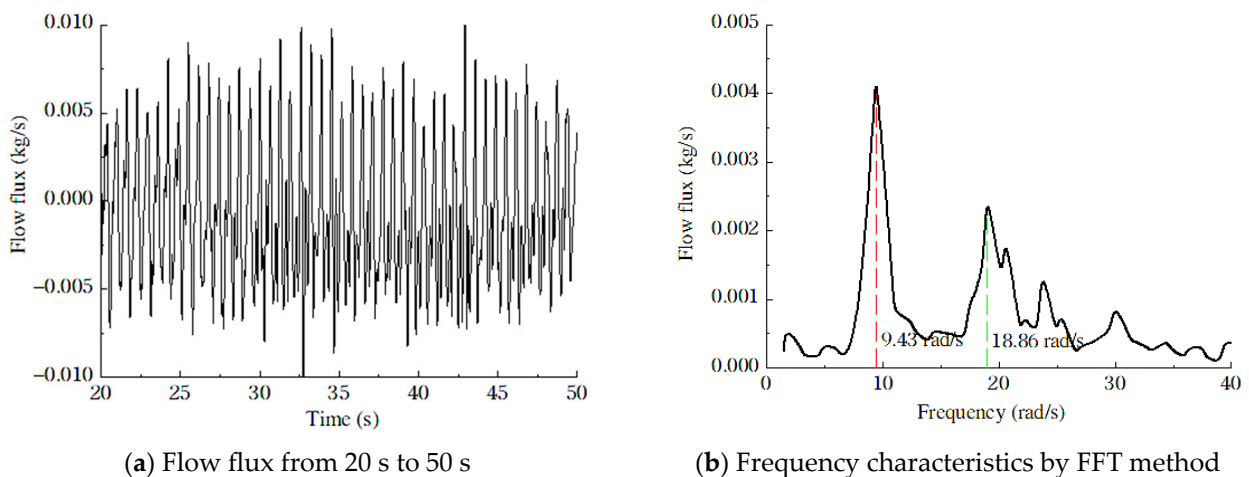


Figure 26. Analysis of irregular characteristics of flow flux for 0.646 s wave period.

Furthermore, it can be also found that except for the case of the 0.646 s wave period, the other time-domain curves versus various wave periods can present the law of periodic change. The amplitude of the flow flux at holes will be greater, with the increase in the wave period; that is, the exchange rate between the fluid in the tank and the external fluid becomes larger, as the wave period becomes bigger. In order to analyze the reason for the above variation trend, velocity vectors near the hole of two cases with 0.646 s and 1.291 s were studied, as shown in Figure 27. Therein, the velocity vectors correspond to the moment of the maximum inlet velocity through the L_1 hole for 0.646 s and 1.291 s wave periods.

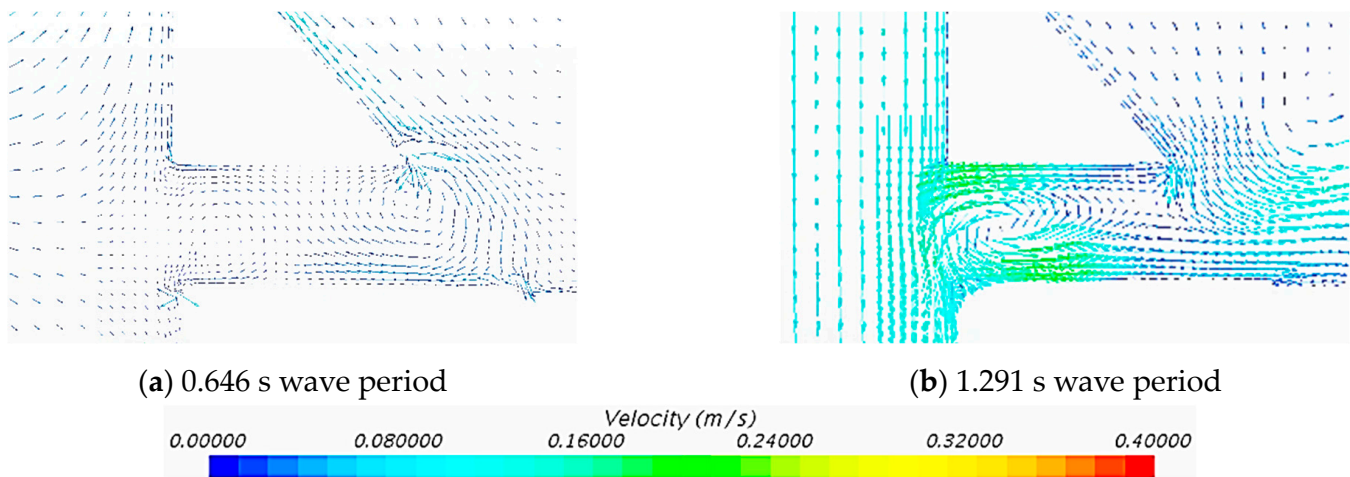


Figure 27. Velocity vectors near the opening hole versus different periods of 0.646 s and 1.291 s.

By comparing the velocity vectors near the opening hole of the vessel versus different periods of 0.646 s and 1.291 s, as demonstrated in Figure 27, it can be seen that the flow velocity of the external fluid mainly comes from the wave action, which makes the fluid flow downward along the vessel wall into the opening hole and then into the fish tank. The shorter the wavelength, the faster the velocity decays with water depth. Thus, the x -directional velocity flowing through the hole in the case with a smaller period (0.646 s) is relatively lower. On the other hand, under the wave condition with a large period (1.291 s), the velocity of the fluid directly flowing into the tank becomes higher. With the increase in the wave period, the exchange of water inside and outside the tank also increases.

3.2. Fluid Characteristics in Fish Tank of a Floating Breeding Vessel with Perforated Broadside

In this section, the characteristics of the fluid field in the fish tank moving with the vessel under the regular wave were further analyzed, and then the influence of motion responses of breeding vessels on the fluid field in the tank was mainly discussed.

3.2.1. Numerical Model of Floating Vessel with Mooring System under Classic Regular Wave

In order to keep the horizontal position of the breeding vessel under the wave condition, the mooring system should be arranged as shown in Figure 28, and mooring tension can be calculated based on the theory of cable dynamics. Therein, the main parameters of the mooring line can be referred to Du (2016), as in Table 10 [26].

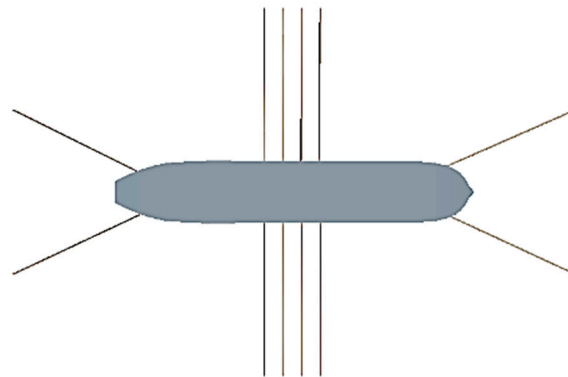


Figure 28. Multi-point mooring system for the breeding vessel.

Table 10. Main parameters of mooring line.

Type	Diameter (mm)	Length (m)	Wet Weight (KN m ⁻¹)	Breaking Strength (KN)	Axial Stiffness (KN)	Pretension (KN)
Anchor chain	2.583	2.28	0.003056	0.0963	8.157	14.58

Furthermore, the wave parameters of the regular wave are listed in Table 11.

Table 11. Main parameters of class regular wave.

Wave Direction	Wave Height <i>H</i> (m)	Water Depth <i>D</i> (m)	Wave Period <i>T</i> (s)	Wave Length λ (m)
90°	0.070	1.267	1.291	2.610

3.2.2. Influence of Motion Responses of a Breeding Vessel on Fluid Field in Fish Tank

Using the above method, the external fluid field outside the vessel with six DOF motions, the internal fluid field in the fish tank, and the interactive flow of the two fields through opening holes under the wave condition were numerically simulated.

Motion responses of the vessel with and without opening holes under the mooring system were calculated and are shown in Figure 29. For roll, pitch, and heave, the curves of motion response only present the periodic characteristics with wave frequency. The time-domain curves of surge, sway, and yaw motions have dual-frequency periodical variations in wave frequency and low frequency. Moreover, the ranges of six DOF motions for the practical scale were -10° to 11° (roll), -0.8° to 0.8° (pitch), 0.2° – 0.8° (yaw), -0.3 to 0.1 m (surge), 0.0 – 2.4 m (sway), and -1.5 to 1.2 m (heave), respectively. Therein, the response of roll motion of the breeding vessel in the beam sea is most pronounced. Furthermore, the holes and sloshing phenomenon in the fish tank have little effect on the motion responses of the vessel. On this basis, the results of the case with holes should be a little bigger than that without holes.

The time-domain flow flux at each opening hole was calculated and is plotted in Figure 30. It can be found that the curve of the flow flux at each opening is accompanied by periodic variations, and there are some differences between the five holes on the same side. Furthermore, comparing the holes on the left and right sides, the flow rate of the right hole is always positive, and the flow rate of the left hole is always negative, which shows that the right opening on the side-facing wave is always in the inflow state and the left opening on the other side is always in the outflow state. The conclusion is quite different from the flow flux of each hole on the fixed vessel, which results from the roll motion response of the vessel subjected to the same wave.

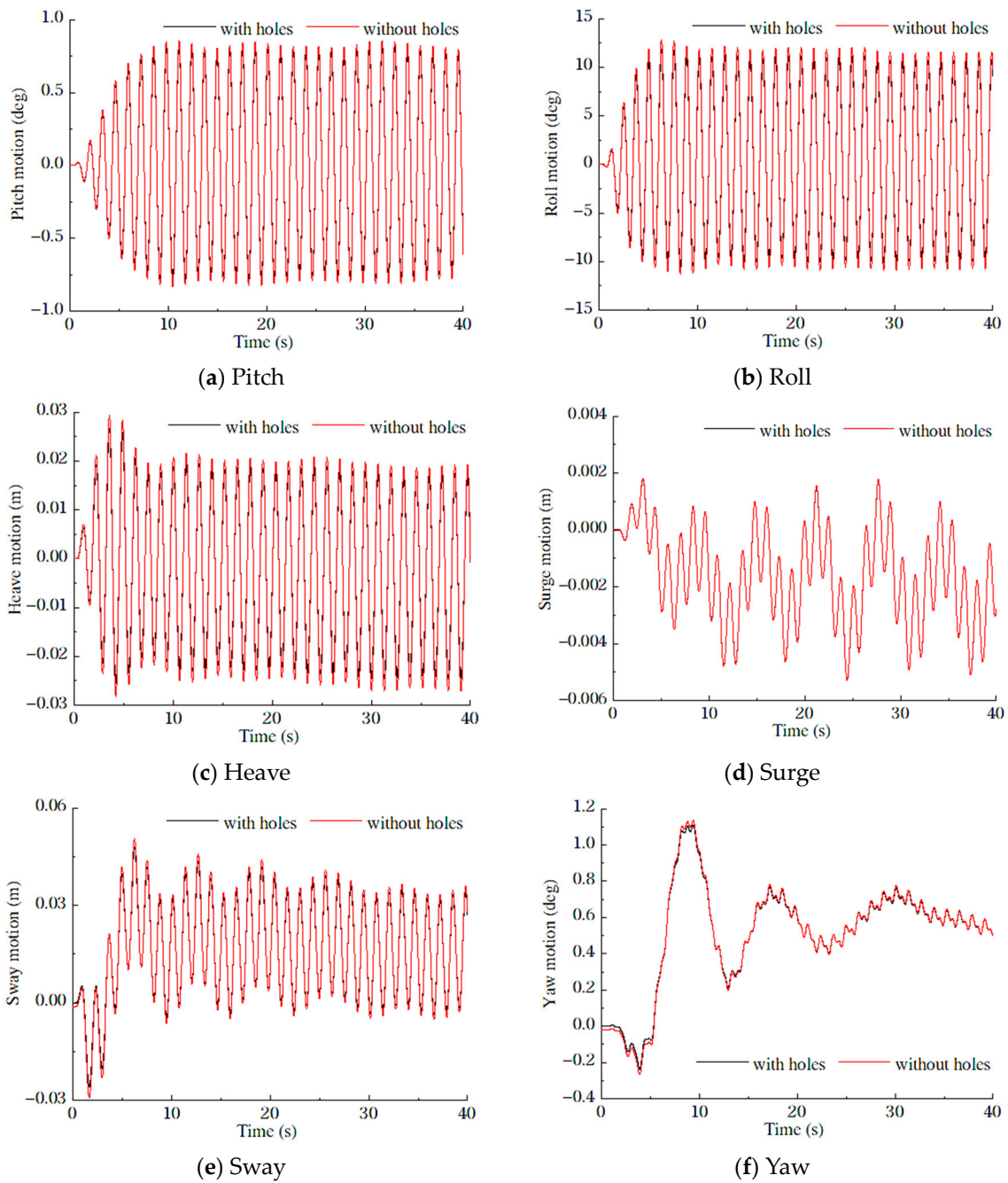


Figure 29. Motion responses of the breeding vessel under the wave condition.

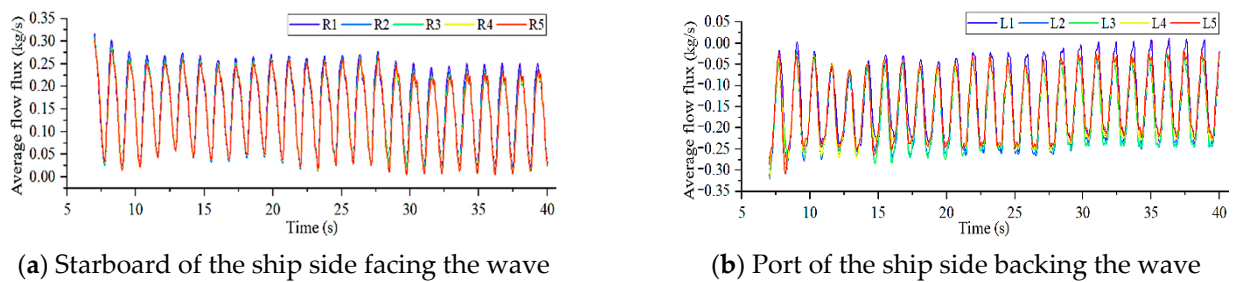


Figure 30. Average flow flux at each opening hole of the breeding vessel under wave action.

Moreover, the characteristics of the free surface and fluid field in the fish tank were numerically simulated. Firstly, the sloshing phenomenon and wave surface along the central axis in the z-direction can be achieved and are shown in Figures 31 and 32. It can be found that the amplitude of the wave elevation presents periodic changes, which is caused by the sloshing phenomenon due to the periodical motion of bulkheads of the fish tank.

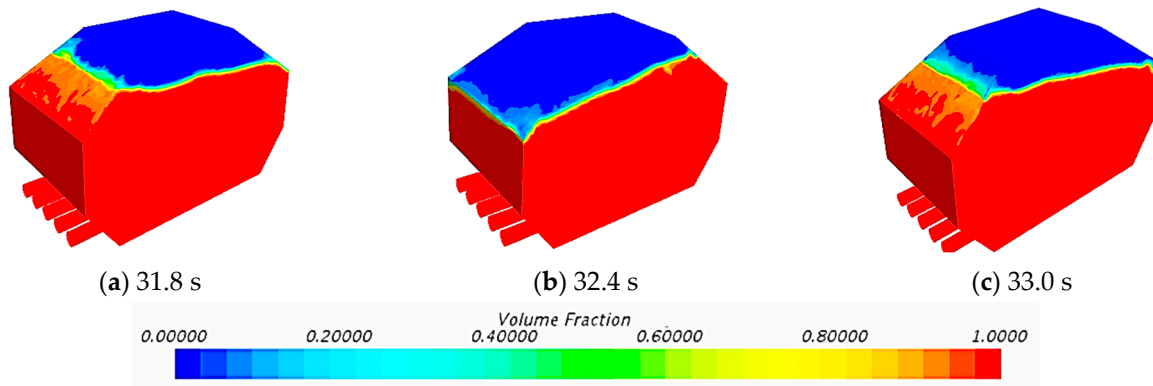


Figure 31. Sloshing phenomenon in the fish tank during a classic period.

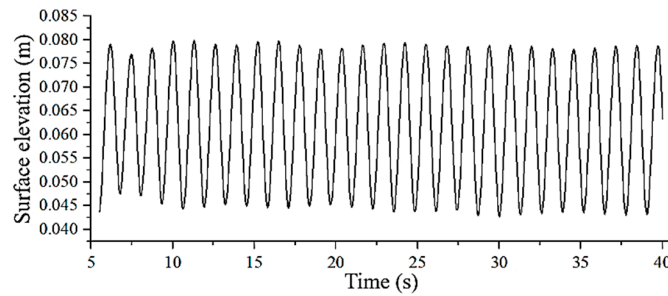


Figure 32. Wave surface along central axis in z direction in fish tank.

With the motions of the fish tank and the breeding vessel, the evolution of a fluid field in the tank due to the sloshing effect of moving bulkheads and external waves through opening holes can be obtained and is plotted in Figure 33.

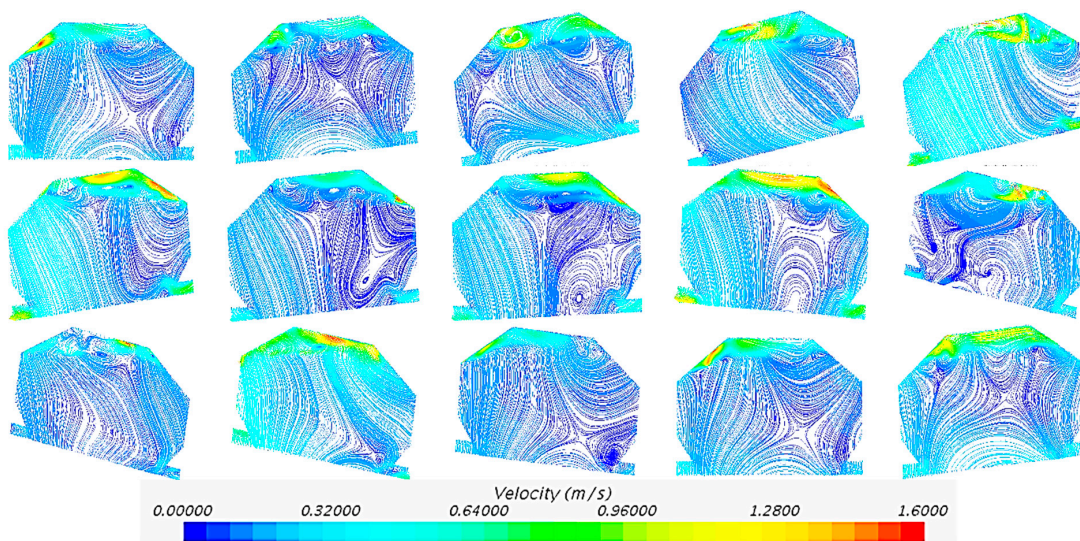


Figure 33. Evolution of fluid field in fish tank of the breeding vessel (26.0–27.4 s, interval 0.1 s).

For a steady periodic process, at its beginning, the initial moment can be chosen as the horizontal state. At this time, the opening holes on both sides of the tank are in a non-flowing state. When the wave crest begins to contact the vessel, the vessel gradually produces the roll motion to the left, driving the fluid in the tank to slosh with the bulkhead. The water at the bottom of the tank will gradually flow toward the left opening and outflow through the hole. As the responses of roll and heave motions increase, the fluid field in the tank produces lateral sloshing and, meanwhile, moves upward as a whole. But part of the fluid on the upper tank will move up along the left wall toward the top and then fall, so that at the free surface, there will be a vortex caused by the fluid falling from the top. With the roll motion toward the horizontal state, the vortex gradually moves down the right bulkhead to the opening holes. Then, as the wave trough gradually touches the vessel, the vessel begins to roll to the right, and the fluid inside the tank gradually begins to move upward along the right side so that the fluid near the vortex at the right opening gradually moves upward and spreads the vortex. When the tank rolls toward the right to a certain angle, a vortex is formed in the right opening hole to block the outflow of fluid in the tank. Because the fluid cannot flow out, a smaller vortex created by the motion of the tank was created at the right opening. Finally, as the fish tank gradually returns to the horizontal position, the vortex gradually spreads out with the fluid sloshing inside the tank and returns to its initial state. From the above whole process, it can be concluded that the fluid field in the fish tank of the breeding vessel is mainly affected by the roll motion response of the vessel.

Moreover, the other test case of the vessel with the same open-hole tank and larger roll inertia moment of the vessel was discussed. Therein, the roll inertial moment changed from about 50 kgm^2 to 100 kgm^2 . Then, its motion responses in the wave can be numerically simulated and are shown in Figure 34. The ranges for practical scale are -5° to 4° (roll), -0.6° to 0.6° (pitch), -0.3° to 0.1° (yaw), -0.36 to 0.00 m (surge), -1.5 to 0.6 m (sway), and -1.5 to 1.2 m (heave), respectively. Therein, the roll motion decreases significantly.

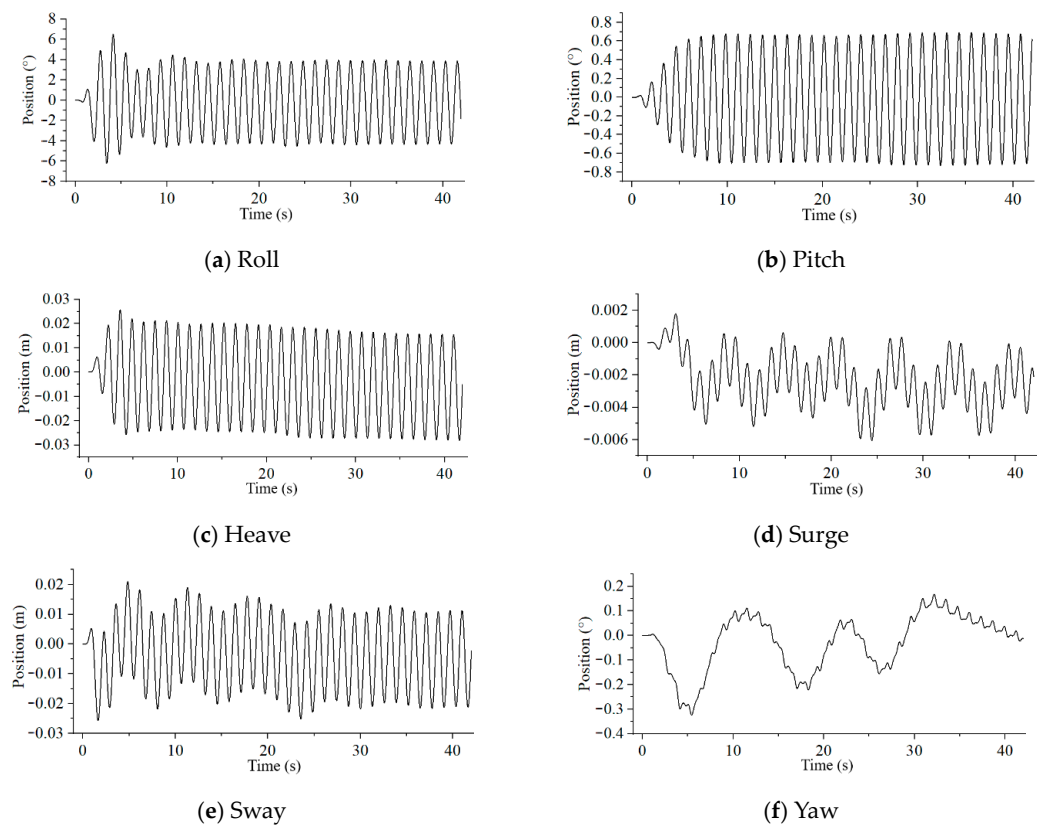


Figure 34. Motion responses of the vessel with larger roll inertia moment under the wave condition.

Subsequently, the average flow flux at each opening hole was monitored, as shown in Figure 35. The time history curves of the flow flux are also accompanied by periodic changes, which are greatly different from those of the vessel with a large roll response. From the figure, the average flow rate of each opening alternates between positive and negative. Therein, the maximum value of the inflow through the right hole is greater than that of the outflow, and the left hole is the opposite, so it can be seen that the roll motion of the vessel has a greater influence on the flow flux through opening holes.

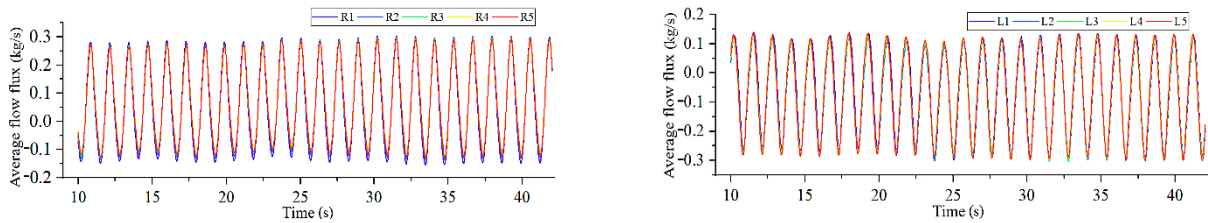


Figure 35. Flow flux through each opening hole of the new vessel with larger roll inertia moment.

In order to analyze the influence of motion responses of the vessel on the flow flux, the total inflow and outflow of three cases, including fixed vessel, small roll response of the vessel with larger inertia moment, large roll response of the vessel with smaller inertia moment, were calculated and are listed in Table 12. From the table, it can be seen that with the roll motion response increasing, the total flow flux gradually becomes larger.

Table 12. Total inflow and outflow through opening holes versus different roll responses.

	Total Inflow (kg)	Total Outflow (kg)	Relative Difference
Fixed vessel	5.446	−5.532	1.58%
Vessel with larger inertia	6.165	−5.946	3.55%
Vessel with smaller inertia	7.711	−7.855	1.88%

Furthermore, the fluid field in the fish tank of the breeding vessel with the larger roll inertia moment can be simulated and is shown in Figure 36.

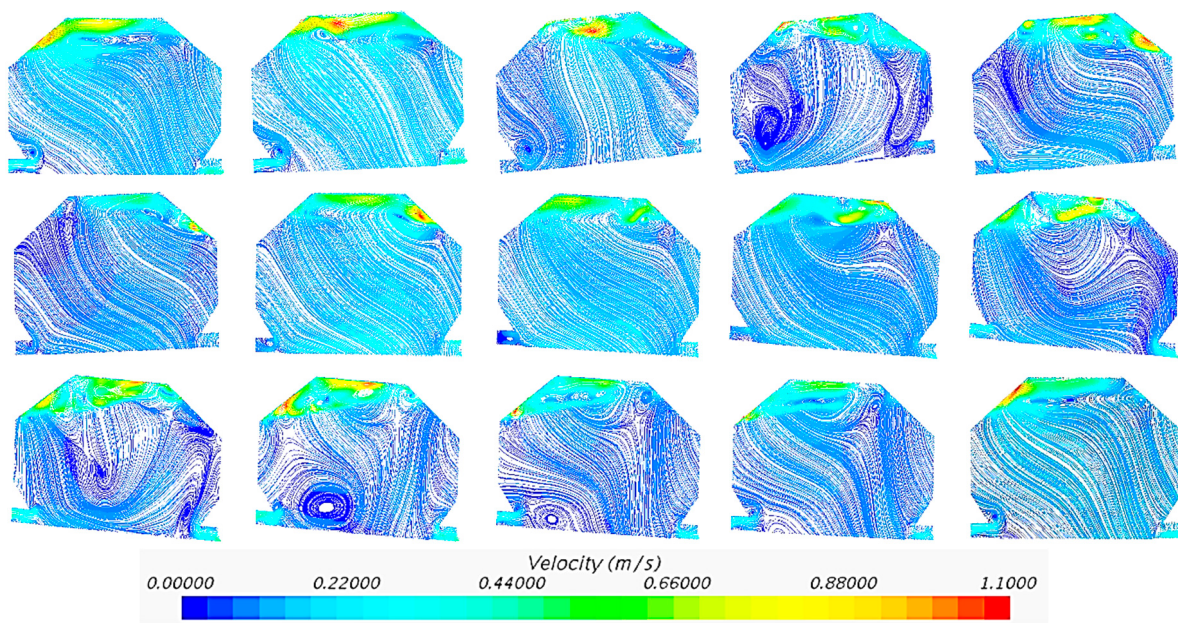


Figure 36. Evolution of fluid field in tank of the vessel with larger roll moment (40.6–42.0 s, interval 0.1 s).

At the beginning of this period, the vessel is in a horizontal position. Meanwhile, the left opening of the tank is in an inflow state, the right opening is in an outflow state, and a vortex near the left opening is created due to the inflow of external fluid. With the vessel subjected to the wave gradually rolling to the left, the state at the opening changes to the left side flowing out and the right side flowing in. The water inside the fish tank is driven to sloshing with the roll motion of the tank, which gradually moves upward to the upper left, up along the left wall of the tank to the top, and then down. So, at the free surface, there is a vortex created by the fluid falling from the top, and the vortex on the left side gradually increases. As the roll returns to the horizontal position, the vortex gradually spreads. Furthermore, the vessel starts rolling to the right, causing the fluid in the tank to gradually develop a tendency to move upward to the right. The still unextinguished leftward action and the newly generated rightward driving effect cause the inner fluid fields to come together, and then a vortex in the middle of the tank appears. Next, the fluid in the tank moves along the right bulkhead to the top and then falls, which produces a vortex at the free surface. Meanwhile, the flow state through opening holes turns again into inflow from the left, and outflow from the right. Finally, as the vessel rolls again to a horizontal position, the vortex gradually disperses, and the inner fluid field returns to the initial flow state.

4. Conclusions

In this paper, the characteristics of the fluid field in a fish tank of breeding vessels with perforated broadsides under wave conditions were analyzed through numerical simulation. For the fixed breeding vessel, the influence of wave direction, wave height, and wave period on the flow field in the tank was discussed. Furthermore, fluid characteristics in the tank of floating vessels with perforated broadsides were studied. Some meaningful conclusions can be made as follows:

(1) The numerical method in the present study to simulate the fluid field in the fish tank of breeding vessels with perforated broadsides has been verified for mesh convergence. Furthermore, by comparing the numerical results with theoretical solutions and experimental data, the accuracy of the method in simulating key issues, including wave generation, fluid–structure interaction, vessel motion, and sloshing phenomenon in the tank, has been validated.

(2) For the fixed breeding vessel, the external wave can cause the trend of periodic variation in the exchange flow through opening holes and the fluid field in the fish tank. In the condition of a head sea from the bow (wave direction 180°), the flow flux through each opening hole is significantly smaller compared to other wave directions. Furthermore, the wave condition of oblique propagation from the ship bow can weaken the overall vortexes in the cross-section and the local vortexes near holes on the horizontal plane in the fish tank, which can reduce the obstruction effect to exchange flow through the opening holes. Thus, the flow velocities at opening holes under the 135° wave are slightly more significant than those under the 90° wave. On the other hand, with the decrease in wave height or wave period, the x -directional velocity flowing through the opening holes gradually decreases, indicating a slowdown in the rate of water exchange inside and outside the fish tank.

(3) For the floating breeding vessel, the roll motion of the vessel has the most significant influence on the exchange flux. As the roll amplitude increases, the sloshing effect caused by the moving bulkhead gradually becomes more significant, affecting the field characteristics in the fish tank, which can reduce the flow flux at each opening hole on both side walls. Notably, when the roll amplitude exceeds 10° , the average flow rate through the right hole is always positive (0.0–0.3 kg/s), while the average flow rate through the left hole is always negative (–0.3 to 0.0 kg/s), which shows that the right opening on wave-facing side is continuously in the inflow state, while the left opening on the other side is always in the outflow state. When the roll amplitude drops to around 5° , the flow states of the left and right holes are presented with inflow and outflow, alternatingly. Therein, the maximum

value of the inflow through the right hole is greater than that of the outflow (-0.25 to 0.15 kg/s), and the left hole is the opposite (-0.15 to 0.25 kg/s).

In the future, the influence of random variations in fluctuation amplitude for the irregular wave condition should be further studied. In our follow-up study, we will focus on the numerical results of the fluid field and flow flux in the fish tank of a breeding vessel with perforated broadsides under various irregular waves corresponding to different wave speeds and different 3 h simulation times, and discuss the influence rule of random fluid velocities and ship motions.

Author Contributions: Conceptualization, W.W.; Methodology, M.L.; Software, G.F.; Validation, K.Z.; Formal analysis, K.Z.; Investigation, W.W.; Data curation, M.L. and K.Z.; Writing—original draft, W.W.; Writing—review & editing, M.L., G.F. and Y.H.; Visualization, G.F.; Supervision, Y.H. All authors have read and agreed to the published version of the manuscript.

Funding: This research was funded by financially supported by the National Natural Science Foundation of China (General Program) (Grant No. 52271259), the National Natural Science Foundation of China (Grant No. 51679034), and the Dalian Innovation Team Support Plan in key areas (2019RT12).

Institutional Review Board Statement: Not applicable.

Informed Consent Statement: Not applicable.

Data Availability Statement: Data are contained within the article.

Acknowledgments: The authors are grateful to all organizations that funded the research in this paper.

Conflicts of Interest: The authors declare no conflict of interest.

References

1. Yu, S.X.; Liu, F. Deep-Water Fish Farming Vessels. CN205524848U, 31 August 2016.
2. Yan, J.; Huang, J.; Li, R. A kind of Fish Farming Vessel and Reforming Method for Oil Tanker Modification. CN106240740A, 21 December 2016.
3. Sun, Y.L. Offshore Farming Facilities Based on Bulk Carrier Conversions. CN106035169B, 31 May 2019.
4. Li, R.; Xie, J.B.; Yan, J.; Chen, X.Y. Design and research on the scheme of transforming oil tanker into aquaculture fishing vessel. *China Water Transp.* **2015**, *15*, 7–9.
5. Li, R.; Xie, J.B.; Yan, J.; Chen, X.Y. Feasibility study on the construction of large-scale green mobile aquaculture fishing vessels in the South China Sea. *Sci. Technol. Inf.* **2015**, *13*, 87–89.
6. Zhang, G.F.; An, H.T.; Liu, Y.; Li, M.Z. Economic argumentation model and system design for refitting bulk carrier into aquaculture engineering ship. *Fish. Mod.* **2018**, *45*, 1–5.
7. Cui, M.C.; Jin, J.H.; Huang, W.Y. Discussion about system construction and general technology of aquaculture platform. *Fish. Mod.* **2019**, *46*, 61–66.
8. Cui, M.C.; Wang, Q.; Guo, X.Y. Numerical Analysis of flow field characteristics in a tank of aquaculture vessel under rolling motion. *Shipbuild. China* **2020**, *61*, 204–215.
9. Wang, Q.; Zhang, B.; Zhang, Y. Design Method for Hull Structure of a Large Aquaculture Engineering Vessel. *Ship Eng.* **2020**, *42*, 14–18.
10. Wang, Q.; Li, J.X.; Cui, M.C. Structural design of large aquaculture engineering vessel. *Fish. Mod.* **2020**, *47*, 75–81.
11. Han, B.; Chen, Z.X.; Cui, M.C.; Wang, Q.W.; Wang, Y.F. Stability Design Criteria and Checking Methods of Deep-sea Aquaculture Platform. *Ship Eng.* **2020**, *42*, 30–35.
12. Labatut, R.A.; Ebeling, J.M.; Bhaskaran, R.; Timmons, M.B. Modeling hydrodynamics and path/residence time of aquaculture-like particles in a mixed-cell raceway (MCR) using 3D computational fluid dynamics (CFD). *Aquac. Eng.* **2015**, *67*, 39–52. [[CrossRef](#)]
13. Song, X.F.; Zheng, S.X.; Dong, D.P.; Huang, Z.T. Simulation and verification of the temperature and flow fields of aquaculture fish tank based on CFD technology. *Period. Ocean. Univ. China* **2018**, *48*, 37–44.
14. Cui, M.C.; Wang, Q.W.; Zhang, B. Numerical Analysis on Water Flow Field Characteristics of Aquaculture Vessel under Pitch Motion. *Ship Eng.* **2020**, *42*, 56–60.
15. Cui, M.C.; Zhang, B.; Wang, Q. Analysis of speed ability and power system configuration of 100000 ton aquaculture platform. *Fish. Mod.* **2020**, *47*, 68–74.
16. Xiao, K.L.; Chen, Z.G.; Dai, Y. Numerical Study on Coupling Effect of Multi-tank Sloshing and Ship Motion. *Ship Eng.* **2020**, *42*, 50–54.
17. Xiao, K.L.; Chen, Z.G. Numerical simulation of aquaculture ship motions coupled with tanks sloshing in time domain. *Chin. J. Ship Res.* **2020**, *15*, 136–144.

18. Xu, X.L.; Yang, Y.C. Study on the sloshing measures of the liquid tank of the breeding vessel. *China Water Transp.* **2017**, *17*, 7–10.
19. Gao, R.; Cui, M.C.; Wang, Q.W.; Wang, J. Numerical analysis on roll fish-suitability of aquaculture water tank. *Ship Eng.* **2020**, *42*, 35–42.
20. Fang, Z.; Xu, H.C.; Dai, J.Y. Application and analysis of the Dual-speed Gearbox in Trailing Suction Hopper Dredger. *Ship Ocean. Eng.* **2021**, *50*, 41–45.
21. Wu, J.T.; Chen, Z.G. Coupled Motion of Tank Sloshing and Aquaculture Platform in Regular Beam Sea. *Ship Eng.* **2021**, *43*, 17–23.
22. Liu, C. Study on CFD Numerical Simulation of Flow Field in the Working Tank of a New Type Fishing Ship. Master's Thesis, Dalian University of Technology, Dalian, China, 2019.
23. Irfan, M.A.; Nallayarasu, S.; Bhattacharyya, S. CFD approach to roll damping of ship with bilge keel with experimental validation. *Appl. Ocean Res.* **2016**, *55*, 1–17. [[CrossRef](#)]
24. Gokce, M.K.; Kinaci, O.K. Numerical simulations of free roll decay of DTMB 5415. *Ocean Eng.* **2018**, *159*, 539–551. [[CrossRef](#)]
25. Hirt, C.W.; Nichols, B.D. Volume of fluid (VOF) method for the dynamics of free boundaries. *J. Comput. Phys.* **1981**, *39*, 201–225. [[CrossRef](#)]
26. Du, M. Hydrodynamic Analysis of FPSO with Multi-Point Mooring System in Shallow Waters. Master's Thesis, China University of Petroleum (East China), Qingdao, China, 2016.

Disclaimer/Publisher's Note: The statements, opinions and data contained in all publications are solely those of the individual author(s) and contributor(s) and not of MDPI and/or the editor(s). MDPI and/or the editor(s) disclaim responsibility for any injury to people or property resulting from any ideas, methods, instructions or products referred to in the content.